International Journal of Thermophysics, Vol. 18, No. 1, 1997

Thermodynamic Properties of Seven Gaseous Halogenated Hydrocarbons from Acoustic Measurements: $CHClFCF_3$, CHF_2CF_3, CF_3CH_3, CHF_2CH_3, $CF_3CHFCHF_2$, $CF_3CH_2CF_3$, and $CHF_2CF_2CH_2F$

K. A. Gillis[1]

Received February 7, 1996

Measurements of the speed of sound in seven halogenated hydrocarbons are presented. The compounds in this study are 1-chloro-1,2,2,2-tetrafluoroethane ($CHClFCF_3$ or HCFC-124), pentafluoroethane (CHF_2CF_3 or HFC-125), 1,1,1-trifluoroethane (CF_3CH_3 or HFC-143a), 1,1-difluoroethane (CHF_2CH_3 or HFC-152a), 1,1,1,2,3,3-hexafluoropropane ($CF_3CHFCHF_2$ or HFC-236ea), 1,1,1,3,3,3-hexafluoropropane ($CF_3CH_2CF_3$ or HFC-236fa), and 1,1,2,2,3-pentafluoropropane ($CHF_2CF_2CH_2F$ or HFC-245ca). The measurements were performed with a cylindrical resonator at temperatures between 240 and 400 K and at pressures up to 1.0 MPa. Ideal-gas heat capacities and acoustic virial coefficients were directly deduced from the data. The ideal-gas heat capacity of HFC-125 from this work differs from spectroscopic calculations by less than 0.2% over the measurement range. The coefficients for virial equations of state were obtained from the acoustic data and hard-core square-well intermolecular potentials. Gas densities that were calculated from the virial equations of state for HCFC-124 and HFC-125 differ from independent density measurements by at most 0.15%, for the ranges of temperature and pressure over which both acoustic and Burnett data exist. The uncertainties in the derived properties for the other five compounds are comparable to those for HCFC-124 and HFC-125.

KEY WORDS: $CHClFCF_3$; CHF_2CF_3; CF_3CH_3; CHF_2CH_3; $CF_3CHFCHF_2$; $CF_3CH_2CF_3$; $CHF_2CF_2CH_2F$; density; equation of state; heat capacity; refrigerants; speed of sound; thermodynamic properties; virial coefficient.

[1] Physical and Chemical Properties Division, Chemical Science and Technology Laboratory, National Institute of Standards and Technology, Gaithersburg, Maryland 20899, U.S.A.

0195-928X/97/0100-0073$12.50/0

1. INTRODUCTION

In 1989, the National Institute of Standards and Technology began an extensive program to measure the thermophysical properties of potential replacements for ozone-depleting refrigerants. Since the inception of this program, high-accuracy acoustic resonance techniques [1–6] have been used to measure the ideal-gas heat capacity C_p° and low-order coefficients for the virial equation of state for these compounds. These results together with accurate measurements of liquid density, vapor pressure, dipole moment, heat capacity, transport properties, surface tension, critical point, and Burnett measurements have been incorporated into the computer program REFPROP [7].

Our laboratory has demonstrated the use of high-accuracy acoustic resonance techniques to determine C_p° and the second and third virial coefficients (B and C, respectively) for a variety of gases [8–14]. These techniques utilize the acoustic resonances of a gas in a small spherical or cylindrical cavity to measure the speed of sound $u(T, p)$ with an uncertainty of 0.01% corresponding to two standard deviations (2σ). From the zero-pressure limit of the speed of sound, the ideal-gas heat capacity C_p° was determined with a 2σ uncertainty of about 0.1%. The pressure dependence of the acoustic data was analyzed with the aid of a model two-body potential to determine coefficients for the virial equation of state. For all these measurements, the limiting factor in the measurement accuracy was the extent to which the gas composition could be measured and maintained.

The results presented in this paper were obtained from measurements performed with an all-metal cylindrical resonator that was described in previous publications [11–14]. When this resonator was used, the test gas came in contact with stainless-steel, gold, and nickel surfaces only. Thus, we made every effort to avoid contaminating the gaseous samples. Furthermore, the acoustic transducers were located outside of the thermostatic fluid bath, near ambient temperature, where they would not be adversely affected by the extreme bath temperatures. Thin metal diaphragms and argon-filled waveguides provided the acoustic coupling between the sample and the remote transducers. This resonator design extended the temperature range over which accurate acoustic measurements could be performed to over 400 K, and it broadened the scope of compounds for which these measurements were possible [11, 14].

By analogy with the virial equation of state, the speed of sound in dilute gases can be represented by an expansion about the ideal-gas limit [6]. In this work, we measure u as a function of the pressure p and the temperature T. Thus, the expansion is written

$$u^2(T, p) = (RT\gamma^\circ/M)[1 + (\beta_a/RT)\, p + (\gamma_a/RT)\, p^2 + (\delta_a/RT)\, p^3 + \cdots] \quad (1)$$

where γ°, β_a, γ_a, and δ_a are functions of the temperature T only. In Eq. (1) R is the universal gas constant,[2] M is the molar mass, and $\gamma^{\circ} = C_p^{\circ}/C_I^{\circ}$ is the ratio of the isobaric to the isochoric ideal-gas heat capacity. We deduce γ° by fitting Eq. (1) to our data, and C_p° is determined from the thermodynamic identity

$$C_p^{\circ} = R\gamma^{\circ}/(\gamma^{\circ} - 1) \tag{2}$$

In Eq. (1), β_a, γ_a, and δ_a are the second, third, and fourth *acoustic* virial coefficients, respectively. If the virial equation of state is written as an expansion in the molar volume V, i.e.,

$$pV/RT = 1 + (B/V) + (C/V^2) + (D/V^3) + \cdots \tag{3}$$

then the coefficients of Eq. (1) and Eq. (3) are related by a set of second-order differential equations [15]. The equations for β_a and γ_a are

$$\beta_a = 2B + 2(\gamma^{\circ} - 1)\, T \frac{dB}{dT} + \frac{(\gamma^{\circ} - 1)^2}{\gamma^{\circ}} T^2 \frac{d^2B}{dT^2} \tag{4}$$

and

$$RT\gamma_a + B\beta_a - \frac{(\gamma^{\circ} - 1)}{\gamma^{\circ}} \left(B + (2\gamma^{\circ} - 1)\, T \frac{dB}{dT} + (\gamma^{\circ} - 1)\, T^2 \frac{d^2B}{dT^2} \right)^2$$
$$= \frac{(1 + 2\gamma^{\circ})}{\gamma^{\circ}} C + \frac{(\gamma^{\circ})^2 - 1}{\gamma^{\circ}} T \frac{dC}{dT} + \frac{(\gamma^{\circ} - 1)^2}{2\gamma^{\circ}} T^2 \frac{d^2C}{dT^2} \tag{5}$$

The corresponding relationships for the higher-order coefficients, δ_a and ε_a (the fifth acoustic virial coefficient), were used in this work; however, they are not given here. These relationships, derived with a symbolic mathematics computer program, will be included with a detailed discussion of higher-order acoustic virial coefficients in a future publication [16]. Note that the equation relating δ_a to the virial coefficients in Ref. 15 is incorrect. When accurate acoustic measurements and accurate p–V–T data for initial conditions are available, the virial coefficients obtained by integrating Eqs. (4) and (5) will have an imprecision comparable to or lower than those determined from conventional p–V–T measurements.

Trusler and Zarari [17] have shown that gas densities and isobaric heat capacities may be determined by numerical integration of accurate sound-speed data. This method requires additional information, e.g., the

[2] The value of the universal gas constant used in this work is 8.314471 J · mol^{-1} · K^{-1} from Ref. 5.

compression factor Z and $(\partial Z/\partial T)_P$ for one isotherm, to provide the initial conditions for the integration. In order to avoid an accumulation of errors as the integration proceeds, they showed that the initial conditions should be specified for the lowest temperature isotherm for which there is acoustic data. However, Z and $(\partial Z/\partial T)_P$ were not available for most of the compounds studied in this work; thus, we could not use the Trusler–Zarari scheme.

Alternatively, parametrized expressions for $\beta_a(T)$, $\gamma_a(T)$, etc., may be fit to the acoustic data through the use of Eq. (1) and the differential equations Eqs. (4) and (5). A physically motivated scheme for obtaining suitable parametrized expressions for $\beta_a(T)$ and $\gamma_a(T)$ is to approximate the intermolecular potential with a hard-core square-well (HCSW) potential [18] defined by

$$U(r) = \begin{cases} \infty, & r < \sigma \\ -\varepsilon, & \sigma < r < \lambda\sigma \\ 0, & r > \lambda\sigma \end{cases} \tag{6}$$

This potential has the essential features of a real intermolecular potential. In Eq. (6) r is the distance between molecular centers, ε is the well depth, σ is the hard-core radius, and λ is the ratio of the width of the well to the width of the hard core. The virial coefficients of a hypothetical gas obeying Eq. (6) have a temperature dependence that closely approximates real gases. The virial coefficients are

$$B(T) = b_0[1 - (\lambda^3 - 1)\,\Delta] \tag{7}$$

and

$$C(T) = \tfrac{1}{8} b_0^2 (5 - c_1\,\Delta - c_2\,\Delta^2 - c_3\,\Delta^3) \tag{8}$$

with

$$\left.\begin{aligned} c_1 &= \lambda^6 - 18\lambda^4 + 32\lambda^3 - 15 \\ c_2 &= 2\lambda^6 - 36\lambda^4 + 32\lambda^3 + 18\lambda^2 - 16 \\ c_3 &= 6\lambda^6 - 18\lambda^4 + 18\lambda^2 - 6 \end{aligned}\right\} \quad \text{for} \quad 1 \leqslant \lambda \leqslant 2$$

or

$$\left.\begin{aligned} c_1 &= 17 \\ c_2 &= -32\lambda^3 + 18\lambda^2 + 48 \\ c_3 &= 5\lambda^6 - 32\lambda^3 + 18\lambda^2 + 26 \end{aligned}\right\} \quad \text{for} \quad \lambda \geqslant 2$$

where

$$\Delta = e^{\varepsilon/k_B T} - 1 \tag{9}$$

Here $b_0 = \frac{2}{3}\pi N_a \sigma^3$, N_a is Avogadro's number, and k_B is Boltzmann's constant. A closed-form expression for the fourth virial coefficient D has been calculated [19] only for certain specific values of λ, namely, 1.1, 1.5, and 2.0. The parameters b_0, λ, and ε are treated as adjustable parameters in the analysis of experimental data. In the work described here, acceptable fits to the acoustic data were obtained with a fixed value of $\lambda = 2.0$ in the square-well form for D. Note that the virial coefficients for a HCSW fluid approach positive constants in the high-temperature limit, $k_B T \gg \varepsilon$, consistent with the hard-sphere limit. Fortunately, this unrealistic feature of the model is benign since ε falls in the range $300 < \varepsilon < 500$ K, and the condition $k_B T \gg \varepsilon$ does not occur at temperatures where these gases are stable.

The virial coefficients that are obtained from the analysis of the acoustic data and the HCSW potential may be used to calculate the gas density. Gas

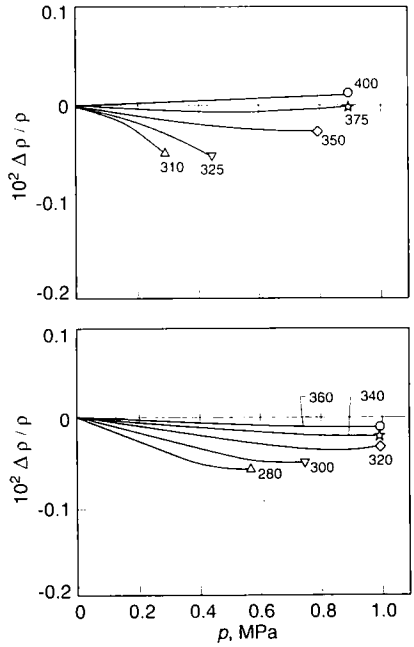

Fig. 1. The densities of (top) HCFC-124 and (bottom) HFC-125 as determined by Burnett measurements compared with indirect determinations from this work. $\Delta\rho/\rho \equiv (\rho_{\text{Burnett}} - \rho_{\text{acoustic}})/\rho_{\text{acoustic}}$.

Table I. Summary of Experimental Conditions and Parameters Used in Eq. (11) for Each Compound

Compound	T range (K)	p max. (MPa)	M (kg·mol^{-1})	T_c (K)	p_c (kPa)	μ (D)	a^* (kg$^{1/2}$·K·Pa^{-1}·s^{-1})
HCFC-124	250–400	0.9	0.136477	395.65	3660.0	1.469	29.04
HFC-125	240–400	1.0	0.120022	339.45	3630.6	1.563	23.44
HFC-143a	250–400	1.0	0.084041	346.25	3811.0	2.340	—
HFC-152a	240–400	1.0	0.066051	386.70	4492.0	2.262	20.63
HFC-236ea	267–377	0.6	0.152039	415.25	3692.2	1.210	30.57
HFC-236fa	276–400	1.0	0.152039	398.07	3219.2	—[a]	30.17
HFC-245ca	311–400	0.9	0.134049	451.55	3855.0	1.777	29.91

[a] Not available.

densities determined from acoustic measurements differed from direct measurements with the Burnett method by at most 0.15%, over the ranges of temperature and pressure for which both measurements exist (see Fig. 1). Thus, the heat capacity and the gas density may be determined *simultaneously* from one sample and one apparatus with an accuracy that is sufficient for many applications.

In this paper, measurements of the speed of sound in seven gaseous halogenated hydrocarbons are presented. The compounds that were studied are 1-chloro-1,2,2,2-tetrafluoroethane ($CHClFCF_3$ or HCFC-124),[3] pentafluoroethane (CHF_2CF_3 or HFC-125), 1,1,1-trifluoroethane (CF_3CH_3 or HFC-143a), 1,1-difluoroethane (CHF_2CH_3 or HSC-152a), 1,1,1,2,3,3-hexafluoropropane ($CF_3CHFCHF_2$ or HFC-236ea), 1,1,1,3,3,3-hexafluoropropane ($CF_3CH_2CF_3$ or HFC-236fa), and 1,1,2,2,3-pentafluoropropane ($CHF_2CF_2CH_2F$ or HFC-245ca). The sound-speed data are given in Tables A1 through A7 in the Appendix. The experimental conditions under which each compound was studied are summarized in Table I. Ideal-gas heat capacities, acoustic virial coefficients, and coefficients for the virial equation of state were determined from these measurements. Comparisons of these measurements with other available high-quality data show excellent agreement. Heat capacities that were calculated from spectroscopic data agree to within 0.2% (see Fig. 7). measurements of the second virial B from p–V–T techniques agree with the present measurements to better than 0.6% (see Figs. 5 and 8). Figure 1 shows that the densities of gaseous HCFC-124 and HFC-125 determined

[3] The nomenclature used to refer to these compounds has been adopted by the refrigeration industry.

from acoustic measurements and the square-well model potential alone differ from density measurements using the Burnett method by at most 0.15%. We emphasize that these gas densities were obtained without any p–V–T data whatsoever.

2. APPARATUS AND PROCEDURES

The acoustic apparatus consisted of a cylindrical resonator, electroacoustic transducers, acoustic waveguides, and diaphragm separators as illustrated in Fig. 2. Details of the construction, the acoustic model, and the performance of this apparatus have been described elsewhere [13, 14]. All of the surfaces in the resonator and in the gas handling system that were in contact with the sample were either stainless steel, gold, or nickel. Since the electroacoustic transducers were remote, they were not influenced by

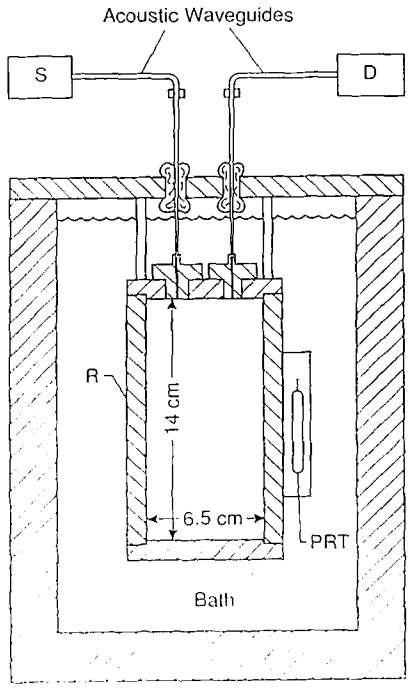

Fig. 2. Diagram of the acoustic apparatus showing the stirred fluid bath, the cylindrical resonator (R), the platinum resistance thermometer (PRT), the acoustic waveguides, and the source (S) and detection (D) electroacoustic transducers.

the bath temperatures. Sound was transmitted between the resonator and the remote transducers through argon-filled acoustic waveguides. The argon gas in the waveguides and the sample in the resonator were separated by thin metal diaphragms whose vibration coupled the sound from the argon to the test gas. To minimize the stress on the diaphragms. the argon pressure was regulated to equal the sample pressure within ± 1 kPa.

The resonator was placed in a temperature-controlled stirred-fluid bath which provided rapid thermal equilibration and a stability of 1 mK. A glass-encapsulated, 25-Ω standard platinum resistance thermometer (SPRT) manufactured by Leeds and Northrop (LN 1818362)[4] was enclosed in an aluminum block attached to the outside of the resonator. Four-wire resistance measurements were performed with a Hewlett–Packard 3458A high-precision ($8\frac{1}{2}$-digit) dc multimeter. All temperatures are reported on ITS-90.

Pressure measurements were made using a Ruska Instrument Corporation Model 6000 DPG (SN 40162), which is a quartz-bourdon-tube differential-type pressure gauge. The reference pressure was kept below 2 Pa with a rotary pump. The gauge's zero-pressure indication was checked and adjusted before each isotherm or about once every 24 h. Between adjustments the zero was observed to drift by as much as 20 pa. From the calibration history of this instrument, the 2σ uncertainty of the indicated pressure was estimated to be $6 \times 10^{-5} p + 20$ Pa by comparison with a standard piston gauge.

Argon was the only gas admitted into the bourdon gauge. A diaphragm-type differential pressure transducer or DPT (MKS Instruments Model 315BD-00100) that separated the sample from the argon buffer gas was used in conjunction with the bourdon gauge to determine the sample pressure. The DPT was made entirely of stainless steel and was bakable to 200°C. A thermostat regulated the temperature of the DPT to within ± 0.1°C of the set point. The set point, chosen for each sample, was high enough to prevent condensation within the DPT over the desired temperature and pressure ranges. The DPT was calibrated at the set-point temperature. The DPT's null indication was checked before each isotherm.

Before the acoustic measurements began, all samples had been degassed at 77 K by repeated freeze–pump–thaw cycles to remove air or

[4] In order to describe materials and experimental procedures adequately, it is occasionally necessary to identify commercial products by manufacturer's name or label. In no instance does such identification imply endorsement by the National Institute of Standards and Technology, nor does it imply that the particular product or equipment is necessarily the best available for the purpose.

other volatile impurities that might be present. Gas chromatographic (GC) analysis provided a standard method of estimating each sample's purity from ratios of peak areas. A sample was deemed to be acceptable if it had a minimum purity of 99.95%. By neglecting an impurity at a molar concentration x, the fractional error in the deduced value of the ideal-gas heat capacity from the measured speed of sound is

$$\frac{\delta C^{\circ}_{p\circ}}{C^{\circ}_{p\circ}} = \left\{ \frac{(C^{\circ}_{pi} - C^{\circ}_{p\circ})}{C^{\circ}_{p\circ}} + \frac{1}{\gamma^{\circ}_{\circ} - 1} \frac{(M_i - M_{\circ})}{M_{\circ}} \right\} x + O(x^2) \qquad (10)$$

where $C^{\circ}_{p\circ}$ and C°_{pi}, are the actual ideal-gas heat capacities of the desired component and the impurity, respectively, $\delta C^{\circ}_{p\circ}$ is the difference between the erroneous, deduced heat capacity and the actual heat capacity of the desired component, $M_{\circ}$ and M_i are the molar masses of the desired component and the impurity, respectively, and $\gamma^{\circ}_{\circ}$ is $C^{\circ}_{p\circ}/C^{\circ}_{v\circ}$. Since $(\gamma^{\circ}_{\circ} - 1)$ was of order 0.1 for the compounds studied here, $\delta C^{\circ}_{p\circ}/C^{\circ}_{p\circ}$ is much more sensitive to the difference in molar masses than it is to the difference in heat capacities. For example, if an impurity is present at a concentration of 0.05% and it has a molar mass that differs from the desired component by 50%, then the error made by neglecting the impurity is about 0.25%.

Each isotherm included measurements of the speed of sound at several pressures. When the bath temperature had stabilized, the resonator was charged with the sample to the highest pressure. After the measurements at one pressure were complete, a quantity of the sample was removed in small steps until the next desired pressure was reached. After each change in pressure, sufficient time was allowed for the temperature of the sample to equilibrate with the bath before beginning the measurements.

Data acquisition and sample manipulation were under automated computer control. The control algorithm included the ability (a) to establish the sample temperature and pressure prescribed by a predetermined set of thermodynamic state points, (b) to record the temperature and pressure at each state point, and (c) to measure the resonance frequency and half-width for a set of chosen acoustic modes. Two 50-ml sample storage vessels, one warm and the other at 77 K, were used to move the sample into and out of the resonator through a series of pneumatic computer-controlled valves. The number of successive isotherms that could be completed automatically depended on the amount of sample available. When all the sample was collected in the cold storage vessel, the program was interrupted while the sample was manually transferred back to the warm vessel. In practice, one isotherm, covering 20 pressures up to 1 MPa, could be completed in a 24-h period.

At each state point, the speed of sound was deduced from the measured resonance frequencies and calculated half-widths of two to four

acoustic modes. For each chosen mode, the signal from the detector was measured at 11 drive frequencies that spanned the full width of the resonance. The data acquisition algorithm swept the frequency through the resonance in both directions to average the systematic effects of small temperature or pressure drifts on the resonance line-shape A frequency synthesizer generated the sinusoidal drive voltage, which was amplified and then fed to the electroacoustic drive transducer. The signal from the acoustic pickup transducer was detected and measured with a two-phase lock-in amplifier. The complex response at the set of chosen frequencies was fit with the theoretically expected six- or eight-parameter function to determine the resonance frequency and half-width. The eight-parameter fit, which includes a complex linear background, was selected only when it was significant at the 97% confidence level. The speed of sound was calculated from the resonance frequency, corrected for the presence of the thermoviscous boundary layer, and the dimensions of the resonator.

The resonator's dimensions were calibrated from acoustic measurements in argon between 240 and 400 K and at pressures up to 1 MPa. As we have noted elsewhere [13, 14], the calibration and test measurements were performed in the same thermostated bath. Thus, the small temperature gradients that are present in the bath when its temperature is far from ambient have negligible effects on the thermodynamic properties deduced from the acoustic results. Typical inconsistencies among the modes were 40 ppm at low pressures and 100 ppm at the highest pressures. The sound speeds determined from the individual modes were averaged together, weighted by the statistical variances between the resonance fits and the data. The statistical variance among the averaged modes was used to weight the speed of sound in the isotherm fits.

The measured resonance frequencies are shifted from those of a hypothetical lossless resonator due to thermoviscous effects [20] near the walls of the resonator. These frequency shifts must be known if the speed of sound is to be determined accurately. An acoustic model of sound propagation in the resonator [6, 13, 14] was used to calculate these shifts from estimates of the transport properties of the gas. (Because the transport properties had not been measured, they were estimated by well-known correlation schemes.) Reichenburg's group-contribution method [21, 22] was used to estimate the dilute-gas viscosity η of each compound. In this method,

$$\eta = \frac{3 \cdot 16 \times 10^{-6} M^{1/2} T}{a^* [1 + 0.36 T_r (T_r - 1)]^{1/6}} \frac{T_r (1 + 270 \mu_r^4)}{(T_r + 270 \mu_r^4)} \tag{11}$$

where η is in Pa·s, a^* is a temperature-independent parameter, M is the molar mass in kg·mol^{-1}, $T_r = T/T_c$, T_c is the critical temperature,

$\mu_r^2 = \mu^2 P_c/(k_B T_c)^2$, μ is the electric dipole moment,[5] P_c is the critical pressure, and k_B is Boltzmann's constant. The value of a^* for each compound (see Table I) was determined by summation of the contributions from each of the functional groups as given in Table 9-3 in Ref. 21. Typically, Reichenberg's method can predict viscosities organic compounds with an error of $\pm 5\%$. A 5% change in the viscosity changes the speed of sound by 20 ppm and changes the ideal-gas heat capacity by 0.02%.

The thermal conductivity was estimated from the modified Eücken correlational [21]:

$$\kappa = \frac{\eta R}{M}[1.32(C_p^\circ/R - 1) + 1.77] \tag{12}$$

where κ is in $W \cdot m^{-1} \cdot K^{-1}$, η is in $Pa \cdot s$, and M is the molar mass in $kg \cdot mol^{-1}$. This method of predicting the thermal conductivity is accurate to about $\pm 20\%$. This uncertainty in the thermal conductivity contributes an uncertainty of about ± 12 ppm in the speed of sound and $\pm 0.01\%$ in the ideal-gas heat capacity.

3. RESULTS

The sound-speed data for each compound are given in Tables A1 through A7. Equation (1) was fitted to the acoustic data on each isotherm by adjusting γ° and the acoustic virial coefficients to minimize χ^2, defined by

$$\chi^2 = \sum_i \frac{[u_i^2 - u^2(T_i, P_i)]^2}{(\sigma_i[u^2])^2} \tag{13}$$

Each point i in the fit was weighted by the statistical variance in the speed of sound among the averaged modes $(\sigma[u_i])^2$. The number of acoustic virial coefficients that were necessary for a proper fit depended on the temperature, the pressure range, and the number of pressures studied. The statistical significance of each coefficient was determined with a Student's t test at the 99.9% level. In no case was a fit higher than order p^4 found to be significant. The tabulated values of C_p°, the acoustic virial coefficients, and the associated 2σ uncertainties are the results from these isotherm fits. The temperature dependence of C_p° was represented by a polynomial expansion in the Celsius temperature t,

$$C_p^\circ/R = a_0 + a_1 t + a_2 t^2 + a_3 t^3 \tag{14}$$

[5] If μ is in Debyes, P_c is in kPa, and T_c is in K, then $\mu_r^2 = \mu^2 P_c/(1.3806 T_c)^2$.

Table II. Coefficients in Eq. (14) for C_p^o (R) from Isotherm Fits

Compound	a_0	$10^2 a_1$ ($°C^{-1}$)	$10^4 a_2$ ($°C^{-2}$)	$10^7 a_3$ ($°C^{-3}$)
HCFC-124	11.240	2.437	−2.130	—
HFC-125[a]	10.769	2.363	−1.430	—
HFC-125[b]	10.766	2.362	−1.420	—
HFC-143a	8.860	2.226	−3.520	1.080
HFC-152a	7.658	1.826	1.031	−0.804
HFC-236ae-I	14.767	2.892	—	—
HFC-236ae-II[c]	14.771	2.957	−1.859	—
HFC-236fa	14.236	3.008	—	—
HFC-245ca	13.177	4.411	−7.872	

[a] Results for the as-received sample and the actual molar mass.
[b] Results for the pure coponent.
[c] Recommended; see Section 3.5.

Equation (14) was fitted to the heat capacity data with each datum weighted by $(3\sigma[C_p^o])^{-2}$, where $\sigma[C_p^o]$ is the standard deviation in C_p^o. The coefficients that were obtained from these fits are given in Table II.

All the isotherms for a compound were combined together to define a surface $u(T, p)$ whose deviations from a fitted correlation were a measure of the internal consistency among the isotherms. A maximum of 12 parameters was adjusted to achieve the best fit to the surface. The correlation, defined by Eqs. (1)–(8) plus the relationships for δ_a and ε_a [16], yielded estimates of B, C, and D that are tabulated in this paper. Higher-order virial coefficients and their temperature derivatives were set to zero, but acoustic virial coefficients through ε_a were always included. Note

Table III. Square-Well Potential Parameters for B, C, and D ($\lambda = 2$ for D in All Cases)

	B			C			D	
Compound	b_0 ($cm^3 \cdot mol^{-1}$)	λ	ε (K)	b_0 ($cm^3 \cdot mol^{-1}$)	λ	ε (K)	b_0 ($cm^3 \cdot mol^{-1}$)	ε (K)
HCFC-124	107.96	1.3320	533.96	170.81	1.7554	190.81	—	—
HFC-125	123.01	1.3241	415.63	258.75	1.1151	575.09	105.60	173.80
HFC-143a	88.22	1.3212	499.59	313.98	1.1514	492.62	16.59	297.30
HFC-142a	66.29	1.3014	632.54	331.53	1.1246	573.65	23.08	317.80
HFC-236ea	284.46	1.3458	384.57	483.09	1.0381	999.31	3.71	700.30
HFC-236fa	265.16	1.3469	386.65	371.75	1.0772	825.52	9.78	469.43
HFC-245ca	258.68	1.3414	427.21	411.51	1.0606	937.79	82.95	282.14

that when the fifth virial coefficient E and its derivatives are zero, no additional adjustable parameters are required to specify ε_a. Although the expressions for B, C, and D were derived from the same square-well potential, a satisfactory fit to the acoustic data was not possible with only one set of potential parameters. Instead, separate sets of potential parameters were assigned to B, C, and D. The parameters were adjusted independently to obtain the best fit. The square-well parameters obtained from the surface fits are given in Table III.

3.1. 1-Chloro-1,2,2,2-tetrafluoroethane (HCFC-124)

The sound-speed measurements in HCFC-124 consisted of 17 isotherms between 250 and 400 K and spanned the pressure range from 20 to 900 kPa. For 12 of the isotherms, the gas handling system was at ambient temperature, and therefore the maximum attainable pressure was

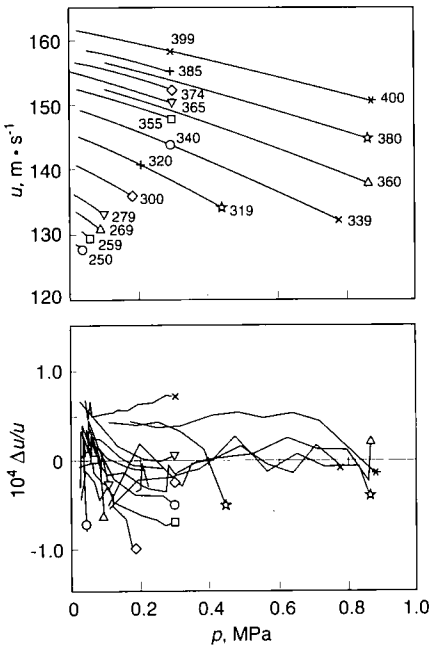

Fig. 3. Top: The speed of sound u in HCFC-124 as a function of p and T. Bottom: The deviations of u from the surface fit described in the text and the coefficients in Tables II and III. The label for each curve is the nominal temperature. $\Delta u/u \equiv (u_m - u_{fit})/u_{fit}$.

325 kPa, which is the vapor pressure of HCFC-124 at 293 K. In order to measure the speed of sound at pressures above 325 kPa, it was necessary to heat the gas handling system above ambient. During these higher pressure measurements, the temperature of all the tubing and valves between the sample storage vessel and the fluid bath was at least 65°C. A thermostat kept the temperature of the DPT at about 65°C and controlled it to within ± 0.1°C. The DPT had been recalibrated under these conditions. Five isotherms between 300 and 400 K represent measurements of the speed of sound at pressures between 100 and 900 kPa (or 60% of the vapor pressure, whichever was lower).

Gas chromatographic analysis, based on peak-area ratios, showed the HCFC-124 sample to be 99.99% pure. The impurities were not identified. The purity was sufficiently high that no corrections to the speed of sound were necessary. Therefore, the molar mass was assumed to be 0.136477 kg mol^{-1} for the analysis of the acoustic data.

The measured speed of sound u and the standard deviation $\sigma[u]$ at each state point are given in Table A1. A plot of u as a function of p for

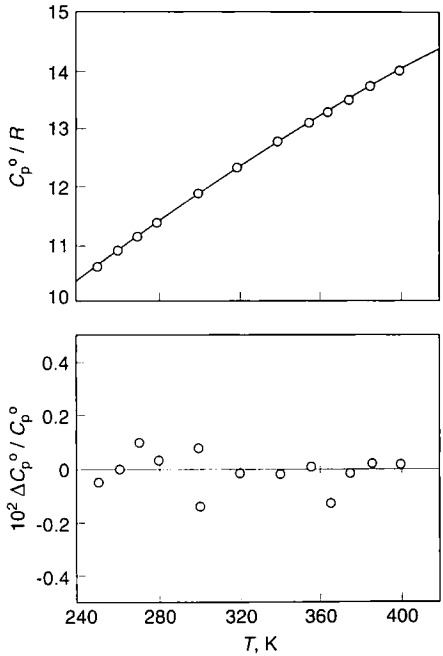

Fig. 4. Top: The measured ideal-gas heat capacity C_p° of HCFC-124 as a function of T. Bottom: The deviations of C_p° from Eq. (14). $\Delta C_p^\circ / C_p^\circ \equiv (C_{p,\mathrm{m}}^\circ - C_{p,\mathrm{fit}}^\circ)/C_{p,\mathrm{fit}}^\circ$.

each isotherm and the deviations of u from the surface fit are shown in Fig. 3. The ideal-gas heat capacity, given in Table IV, was determined from 13 isotherms for which the acoustic data extended to low pressures. Figure 4 shows the measured C_p^o and the deviations from Eq. (14) as a function of T. The acoustic virial coefficients obtained from the isotherm fits are given in Table IV. The surface $u(T, p)$ was fit with nine adjustable parameters. The surface fit included the virial coefficients B and C from which the acoustic virials β_a, γ_a, δ_a, and ε_a were calculated. The coefficients D and E were fixed at zero. Estimates of B and C based on the fitted potential parameters are given in Table IV for several temperatures. Figure 5 shows a plot of $B(T)$ from this work compared with values from p–V–T measurements [23], over the temperature range of the acoustic measurements. The maximum difference between the two independent measurements is only 0.5%.

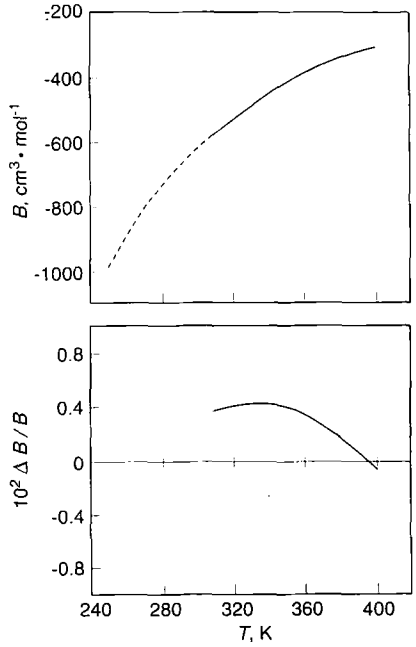

Fig. 5. Top: The second virial coefficient B of HCFC-124 from this work and from p–V–T measurements. Bottom: fractional deviations of p–V–T measurements of B from this work. (----) This work; (——) Ref. 23. $\Delta B/B \equiv (B_{pVT} - B_{acoustic})/B_{acoustic}$.

Table IV. Ideal-Gas Heat Capacity, Acoustic Virial Coefficients, and Density Virial Coefficients for HCFC-124

T (K)	C_p^o (R)	$2\sigma[C_p^o]$ (R)	β_a ($cm^3 \cdot mol^{-1}$)	γ_a ($cm^3 \cdot mol^{-1} \cdot kPa^{-1}$)	$10^5\delta_a$ ($cm^3 \cdot mol^{-1} \cdot kPa^{-2}$)	B ($cm^3 \cdot mol^{-1}$)	$10^{-4}C$ ($cm^6 \cdot mol^{-2}$)
250.010	10.660	0.005	−1509.8	—	—	−990.5	−0.84
259.966	10.915	0.004	−1367.3	—	—	−892.6	0.53
269.908	11.172	0.011	−1255.0	−0.654	—	−809.0	1.50
279.871	11.407	0.009	−1160.3	−0.430	—	−736.6	2.19
300.035	11.863	0.010	−987.9	−0.244	—	—	—
300.043	11.889	0.006	−989.1	−0.245	—	−617.3	3.03
319.675[a]	—	—	−854.9	−0.125	−6.0	—	—
319.675	12.326	0.006	−863.1	−0.091	−10.1	—	—
320.269	—	—	−855.7	−0.127	—	−524.5	3.40
339.740[a]	—	—	−745.8	−0.068	−3.4	—	—
339.740	12.766	0.007	−745.6	−0.067	−3.6	—	—
340.221	—	—	−743.2	−0.081	—	−451.9	3.52
355.095	13.095	0.007	−673.9	−0.053	—	—	—
360.040	—	—	−649.2	−0.045	−1.5	−393.4	3.50
365.000	13.281	0.011	−634.6	−0.033	—	—	—
374.900	13.496	0.008	−592.2	−0.034	—	—	—
380.120	—	—	−567.5	−0.037	—	−344.5	3.42
385.650	13.713	0.013	−555.6	−0.019	—	—	—
399.933	—	—	−505.4	−0.019	—	—	—
400.045	13.991	0.005	−504.3	−0.020	—	−304.0	3.29
400.045[a]	—	—	−505.6	−0.019	—	—	—

[a] Merged isotherm of high- and low-pressure data.

3.2. Pentafluoroethane (HFC-125)

The sound-speed measurements in HFC-125 consisted of nine isotherms between 240 and 400 K and spanned the pressure range from 40 to 1000 kPa (or 0.8 times the vapor pressure, whichever was lower). Since the vapor pressure of HFC-125 at 300 K is well over 1.0 MPa, it was unnecessary to heat the gas handling system to prevent condensation. The tubing and valves were at ambient temperature. The DPT temperature was controlled at 65°C.

The manufacturer's analysis of the HFC-125 sample stated that the most abundant impurity was chloropentafluoroethane (CFC-115). Trace amounts of CO_2 and CO were also present. A quantitative analysis with a GC at NIST that had been calibrated for the sensitivity of CFC-115

showed that the sample contained 99.85% by mole HFC-125 and 0.15% by mole CFC-115. No other impuritites were found with this analysis. This analysis was used to deduce the speed of sound and ideal-gas heat capacity of pure HFC-125 from measurements with the as-received sample. Distillation of the sample was not attempted because CFC-115 and HFC-125 were predicted to form an azeotrope at a composition close to that of the sample. The molar mass of the as-received sample was given by

$$M_m = (1-x)\,M_{125} + xM_{115} = 0.120074\ \text{kg}\cdot\text{mol}^{-1} \tag{15}$$

where M_{125} is the molar mass of pure HFC-125 (0.120022 $\text{kg}\cdot\text{mol}^{-1}$), M_{115} is the molar mass of pure CFC-115 (0.154470 $\text{kg}\cdot\text{mol}^{-1}$), and x is the mole fraction of CFC-115. Throughout the remainder of this sections subscript m refers to the as-received sample, subscript 125 refers to pure HFC-125, and subscript 115 refers to pure CFC-115.

The measured speed of sound u_m, the deduced speed of sound in pure HFC-125 u_{125}, and the standard deviation $\sigma[u]$ at each state point are given in Table A2. Under the assumption that the slight impurity had a negligible effect on the pressure dependence of u_m, the correction applied to u_m was merely a temperature-dependent multiplicative factor:

$$u_{125}^2 = u_m^2 \frac{\gamma_{125}^o}{M_{125}} \frac{M_m}{\gamma_m^o}$$

which, correct to $O(x)$, becomes

$$u_{125}^2 \approx u_m^2 \left\{ 1 - \frac{C_{v125}^o}{C_{v125}^o} \frac{(\gamma_{115}^o - \gamma_{125}^o)}{\gamma_{125}^o} x + \frac{(M_{115} - M_{125})}{M_{125}} x \right\} \tag{16}$$

The determination of C_{p125}^o (and, therefore, C_{v125}^o and γ_{125}^o) is explained below. u_m was lower than u_{125} by about 0.02% over the temperature range studied here. A plot of u_{125} as a function of p for each isotherm and the deviations from the surface fit are shown in Fig. 6. If the presence of the CFC-115 impurity had been entirely neglected and the molar mass of HFC-125 had been used in Eq. (1), then, from Eq. (10), the deduced ideal-gas heat capacity would have been 0.4 to 0.5% too high.

The ideal-gas heat capacities, determined from eight of the nine isotherms, are shown in Table V. Some evidence of changes in the composition were noted during the 400 K isotherm. This isotherm was not included in the determination of the heat capacity. However, the 400 K isotherm above 200 kPa was included in the surface fit. C_{pm}^o was determined from the measured speed of sound u_m with the molar mass given by Eq. (15).

Table V. Ideal-Gas Heat Capacity, Acoustic Virial Coefficients, and Density Virial Coefficients for HFC-125

T (K)	$C^{o}_{p/m}$ (R)	$C^{o}_{p/115}$ (R)	$C^{o}_{p/125}$ (R)	$2\sigma[C^{o}_{p/m}]$ (R)	β_a ($cm^3 \cdot mol^{-1}$)	γ_a ($cm^3 \cdot mol^{-1} \cdot kPa^{-1}$)	$10^5\delta_a$ ($cm^3 \cdot mol^{-1} \cdot kPa^{-2}$)	B ($cm^3 \cdot mol^{-1}$)	$10^{-4}C$ ($cm^6 \cdot mol^{-2}$)	$10^{-8}D$ ($cm^9 \cdot mol^{-3}$)
240.007	9.972	11.409	9.970	0.013	−971.4	−0.371		−632.9	−8.02	−1.353
260.023	10.453	11.989	10.451	0.013	−811.4	−0.168		−518.3	0.58	−0.643
279.988	10.928	12.540	10.925	0.009	−683.8	−0.075	−5.2	−431.7	2.90	−0.311
300.003	11.392	13.070	11.390	0.010	−582.4	−0.040	−2.4	−364.1	3.21	−0.148
319.988	11.850	13.572	11.847	0.009	−499.7	−0.022	−1.0	−310.2	2.93	−0.066
340.003	12.286	14.047	12.283	0.011	−430.7	−0.014		−266.4	2.53	−0.025
359.958	12.709	14.497	12.706	0.005	−373.2	−0.007		−230.2	2.17	−0.004
379.983	13.132	14.922	13.129	0.006	−323.2	−0.002		−199.7	1.88	0.006
400.000								−173.9	1.67	0.011

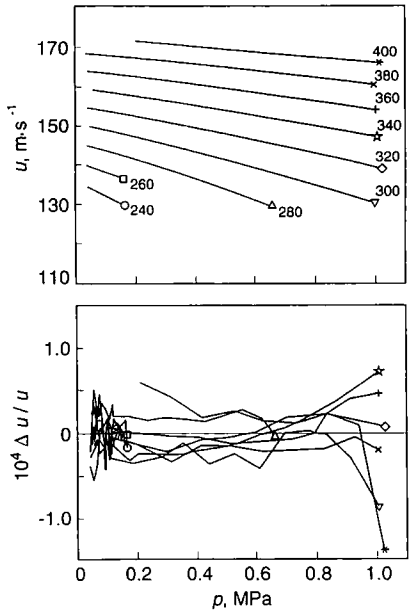

Fig. 6. Top: The speed of sound u_{125} in HFC-125 as a function of p and T. Bottom: The deviations of u from the surface fit described in the text and the coefficients in Tables II and III. The label for each curve is the nominal temperature. $\Delta u/u \equiv (u_m - u_{fit})/u_{fit}$.

Since molar quantities combine as mole fraction averages, C^o_{p125} was given by

$$C^o_{p125} = [C^o_{pm} - xC^o_{p115}]/(1-x) \tag{17}$$

with C^o_{p115} obtained from the program REFPROP. Both C^o_{pm} and C^o_{p125} from Table V were fit with Eq. 14. The results are given in Table II. Figure 7 shows C^o_{p125} and the deviations from Eq. (14) as a function of T. The ideal-gas heat capacity of HFC-125 calculated [24, 25] from spectroscopic data [26, 27] agrees very well with this work (see Table VI). The ideal-gas heat capacity of HFC-125 from $TRC^{(24)}$ differs by 0.9 to 1.7% from earlier calculations by Chen et al. [25]. The vibrational mode assignments given by Compton and Rayner [26], on which the *TRC* calculation is based, are considered to be more reliable than the previous assignments due mainly to the electron diffraction studies by Beagley et al. [27].

Table VI. Comparison of the Ideal-Gas Heat Capacity and Second Virial Coefficient of HFC-125 from this Work with Other Sources

T (K)	C_p° (R)		$10^2 \cdot \Delta C_p^\circ / C_p^\circ$	B ($cm^3 \cdot mol^{-1}$)		
	TRC [24]	This work		This work	Ref. 29	Ref. 28
270.00	—	—	—	−472.2	−475.0	
273.16	10.746	10.766	0.19	—	—	
280.00	—			−431.6	−433.9	—
290.00	—		—	−395.9	−397.7	−395.1
298.15	11.354	11.348	−0.05	—		—
300.00	11.398	11.390	−0.07	−364.1	−365.5	−363.2
310.00		—		−335.7	−336.9	−335.5
330.00	—			−287.2	−288.0	
350.00	—			−247.4	−248.0	
370.00	—	—	—	−214.3	−214.7	—
400.00	13.567	13.534	−0.24	—		

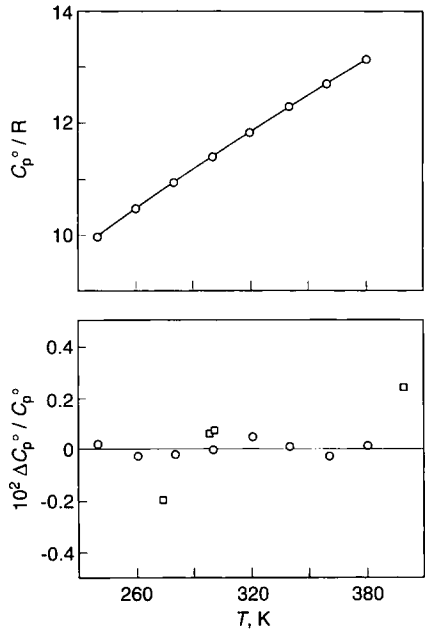

Fig. 7. Top: The measured ideal-gas heat capacity C_p° of HFC-125 as a function of T. Bottom: The deviations of C_p° from Eq. (14). $\Delta C_p^\circ / C_p^\circ \equiv (C_{p,\mathrm{m}}^\circ - C_{p,\mathrm{fit}}^\circ)/C_{p,\mathrm{fit}}^\circ$. The calculated values from Ref. 24 are also shown.

The acoustic virial coefficients obtained from the isotherm fits are given in Table V. The number of coefficients that were significant at the 99.9% level is indicated by the number of entries in the table for each temperature. The surface $u(T, p)$ was fit with 11 adjustable parameters. The surface fit included the virial coefficients B, C, and D from which the acoustic virials β_a, γ_a, δ_a, and ε_a were calculated. The coefficient E was fixed at zero. Estimates of B, C, and D from this work based on the fitted potential parameters are given in Table V for several temperatures. Figure 8 shows a plot of $B(T)$ from this work compared with values from p–V–T measurements [28, 29] given in Table VI, over the temperature range of the acoustic measurements.

3.3. 1,1,1-Trifluoroethane (HFC-143a)

The sound-speed measurements in HFC-143a consisted of eight isotherms between 250 and 400 K and spanned the pressure range from 40

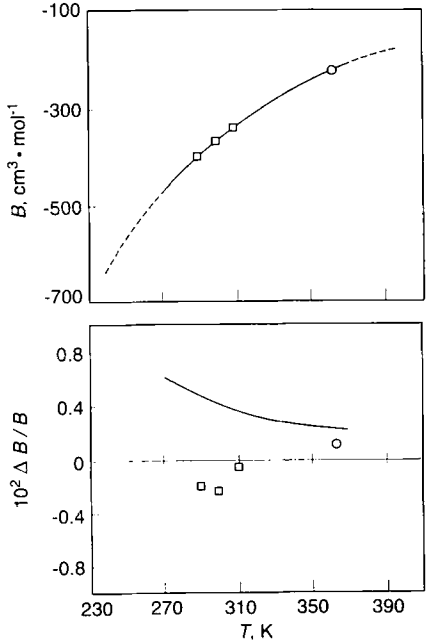

Fig. 8. Top: The second virial coefficient B of HFC-125 from this work and from p–V–T measurements. Bottom: Factional deviations of p–V–T measurements of B from this work. (----) This work; (□) Ref. 28; (——, ○) Ref. 29. $\Delta B/B \equiv (B_{pVT} - B_{\text{acoustic}})/B_{\text{acoustic}}$.

to 1000 kPa (or 0.8 times the vapor pressure, whichever was lower). Since the vapor pressure of HFC-143a at 300 K is about 1.0 MPa, it was necessary to heat the gas handling system to prevent condensation. The temperature of the tubing and valves was maintained at for above 65°C. The DPT temperature was controlled at 65°C. Before the acoustic measurements began, the sample was purified by preparative-scale GC techniques [30]. Gas chromatographic analysis showed the purified sample to be 99.99% pure based on peak area ratios. The impurities were not identified. The purity was sufficiently high that no corrections to the speed of sound were necessary. The molar mass of the sample was assumed to be 0.0840412 kg · mol $^{-1}$. Estimates of the viscosity and thermal conductivity of the gas, used in the analysis of the sound-speed data, were obtained from the predictive program REFPROP Version 4.0.

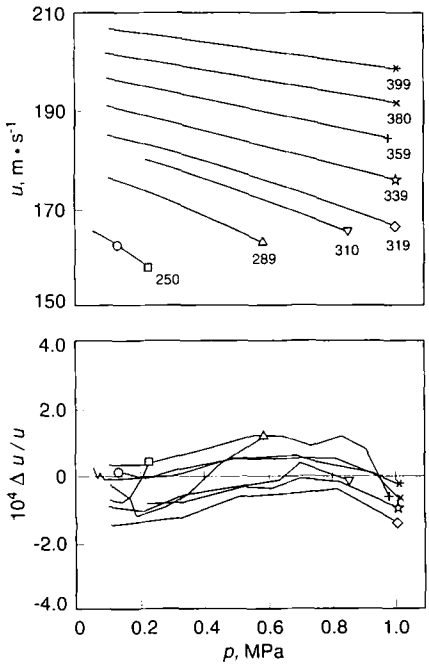

Fig. 9. Top: The speed of sound u in HFC-143a as a function of p and T. Bottom: The deviations of u from the surface fit described in the text and the coefficients in Tables II and III. The label for each curve is the nominal temperature. $\Delta u/u \equiv (u_m - u_{fit})/u_{fit}$.

The measured speed of sound u and the standard deviation $\sigma[u]$ at each state point is given in Table A3. A plot of u as a function of p for each isotherm and the deviations from the surface fit are shown in Fig. 9. The ideal-gas heat capacities, determined from eight isotherms, are shown in Table VII. Figure 10 shows C_p^o and the deviations from Eq. (14) as a function of T. No other measurements were found with which to compare these results. Also given in Table VII are the acoustic virial coefficients, obtained from the isotherm fits, and estimates of B and C based on the fitted potential parameters for several temperatures. No other measurements were found with which to compare these results.

3.4. 1,1-Difluoroethane (HFC-152a)

The sound-speed measurements in HFC-152a consisted of nine isotherms between 243 and 400 K and spanned the pressure range from 40 to 1000 kPa (or 80% of the vapor pressure, whichever was lower). Since

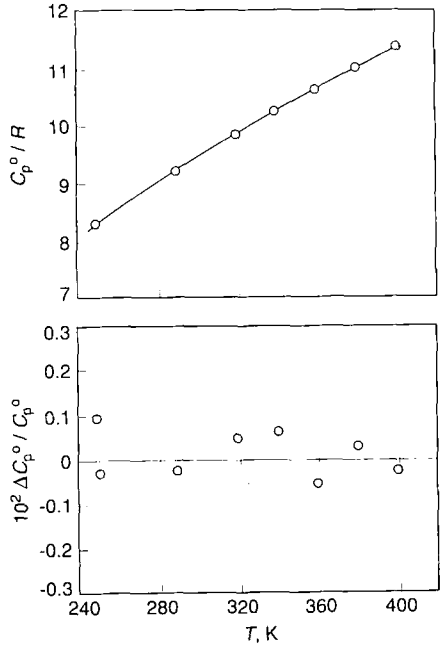

Fig. 10. Top: The measured ideal-gas heat capacity C_p^o of HFC-143a as a function of T. Bottom: The deviations of C_p^o from Eq. (14). $\Delta C_p^o/C_p^o \equiv (C_{p,m}^o - C_{p,fit}^o)/C_{p,fit}^o$.

Table VII. Ideal-Gas Heat Capacity, Acoustic Virial Coefficients, and Density Virial Coefficients for HFC-143a

T (K)	C_p° (R)	$2\sigma[C_p^\circ]$ (R)	β_a ($cm^3 \cdot mol^{-1}$)	γ_a ($cm^3 \cdot mol^{-1} \cdot kPa^{-1}$)	$10^5\delta_a$ ($cm^3 \cdot mol^{-1} \cdot kPa^{-2}$)	B ($cm^3 \cdot mol^{-1}$)	$10^{-4}C$ ($cm^6 \cdot mol^{-2}$)	$10^{-8}D$ ($cm^9 \cdot mol^{-3}$)
250.011	8.333	0.009	−940.5	−0.201	−15.0	−646.3	0.86	−0.447
250.026	8.323	0.005			–	-	-	
289.962	9.223	0.015	−667.4	−0.057	−2.1	−441.9	5.17	−0.115
319.438	9.831	0.019	−534.1	−0.023	−0.5	−347.0	4.58	−0.049
339.913	10.228	0.010	−462.4	−0.011	−0.8	−297.6	3.98	−0.028
359.985	10.593	0.006	−404.1	−0.004	0.0	−258.1	3.47	−0.017
379.998	10.972	0.005	−355.2	0.001	0.1	−225.6	3.05	−0.011
399.979	11.335	0.009	−313.4	0.004	0.1	−198.3	2.74	−0.007

the vapor pressure of HFC-152a at 300 K is 630 kPa, the temperature of all the tubing and valves between the sample storage vessel and the fluid bath was at least 65°C. A thermostat kept the temperature of the DPT at about 65°C and controlled it to within ± 0.1°C. The DPT had been recalibrated under these conditions.

Gas chromatographic analysis, based on peak-area ratios, showed the HFC-152a sample to be 99.99% pure after degassing at 77 K. The impurities were not identified. The sample was sufficiently pure that no corrections to the speed of sound were necessary. Therefore, the molar mass was assumed to be 0.0660508 kg · mol $^{-1}$ for the analysis of the acoustic data.

The measured speed of sound u and the standard deviation $\sigma[u]$ at each state point is given in Table A4. Figure 11 shows a plot of u as a function of p and the deviations from the surface fit for each isotherm. The

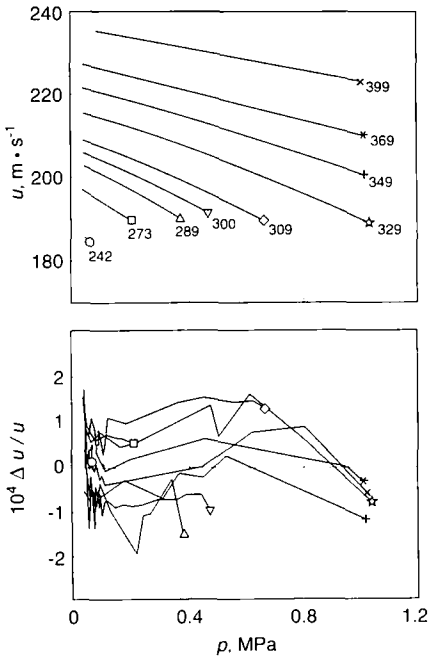

Fig. 11. Top: The speed of sound u in HFC-152a as a function of p and T. Bottom: The deviations of u from the surface fit described in the text and the coefficients in Tables II and III. The label for each curve is the nominal temperature. $\Delta u \, u \equiv (u_m - u_{fit}) \, u_{fit}$.

ideal-gas heat capacities, obtained from the isotherm fits, are given in Table VIII. Figure 12 shows the measured C_p^o and the deviations from Eq. (14) as a function of T. The acoustic virial coefficients, obtained form the isotherm fits, are given in Table VIII. The surface $u(T, p)$ was fit with 12 adjustable parameters. The surface fit included the virial coefficients B, C, and D from which the acoustic virials β_a, γ_a, δ_a, and ε_a were calculated. The coefficient E was fixed at zero. Estimates of B, C, and D based on the fitted potential parameters are given in Table VIII for several temperatures.

3.5. 1,1,1,2,3,3-Hexafluoropropane (HFC-236ea)

The sound-speed measurements in HFC-236ea consisted of 10 isotherms between 267 and 377 K and spanned the pressure range from 40 to 620 kPa (or 80% of the vapor pressure, whichever was lower). Since the vapor pressure of HFC-236ea at 300 K is 220 kPa, the temperature of all the tubing and valves between the sample storage vessel and the fluid bath

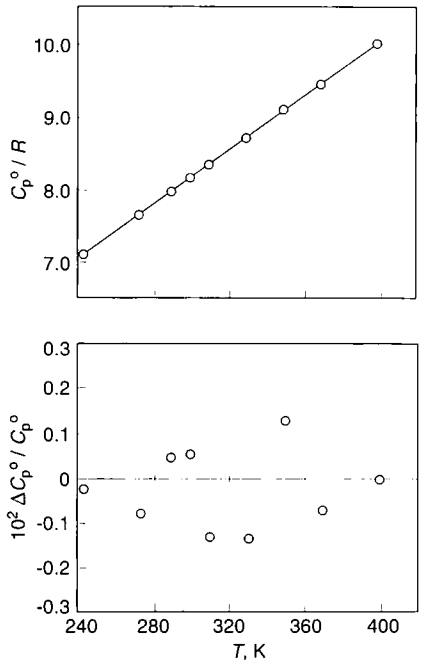

Fig. 12. Top: The measured ideal-gas heat capacity C_p^o of HFC-152a as a function of T. Bottom: The deviations of C_p^o from Eq. (14) ΔC_p^o, $C_p^o \equiv (C_{p,m}^o - C_{p,fit}^o)\, C_{p,fit}^o$.

Table VIII. Ideal-Gas Heat Capacity, Acoustic Virial Coefficients, and Density Virial Coefficients for HFC-152a

T (K)	C_p° (R)	$2\sigma[C_p^\circ]$ (R)	β_a ($cm^3 \cdot mol^{-1}$)	γ_a ($cm^3 \cdot mol^{-1} \cdot kPa^{-1}$)	$10^5\delta_a$ ($cm^3 \cdot mol^{-1} \cdot kPa^{-2}$)	B ($cm^3 \cdot mol^{-1}$)	$10^{-4}C$ ($cm^6 \cdot mol^{-2}$)	$10^{-8}D$ ($cm^9 \cdot mol^{-3}$)
242.776	7.114	0.015	−1306.0			−934.3	−18.84	−3.013
273.130	7.652	0.008	−921.3	−0.178	−22.4	−662.7	2.47	−0.984
289.946	7.971	0.013	−797.3	−0.131		−561.1	4.92	−0.567
300.013	8.159	0.005	−736.7	−0.061	−8.5	−511.1	5.35	−0.416
309.991	8.330	0.010	−683.9	−0.036	−6.2	−468.0	5.40	−0.310
329.945	8.702	0.005	−583.7	−0.031	−2.3	−396.7	4.98	−0.178
349.990	9.098	0.010	−531.3	−0.037	−1.4	−340.3	4.36	−0.105
369.985	9.443	0.005	−452.0	−0.005	--	−295.0	3.77	−0.065
399.959	9.975	0.003	−370.4	−0.004		−242.0	3.09	−0.032

was at least 65°C. A thermostat kept the temperature of the DPT at about 65°C and controlled it to within ±0.1°C. The DPT had been recalibrated under these conditions.

The acoustic measurements were performed on two samples. The sample of HFC-236ea as received from the manufacturer is denoted HFC-236ea-I. Gas chromatographic analysis of HFC-236ea-I, based on peak-area ratios, showed the sample to be 99.8% pure after degassing at 77 K. The impurities were not identified. A small amount of the sample was purified with a preparative-scale GC. The purified sample is referred to as HFC-236ea-II. Analysis of HFC-236ea-II showed it to be 99.99% pure. The measurements below 321 K were obtain from HFC-236ea-II. The measurements at temperatures above 321 K were obtained from HFC-236ea-I.

Since the impurities in HFC-236ea-I were not identified, the corrections applied to those data to account for the impurity must be considered

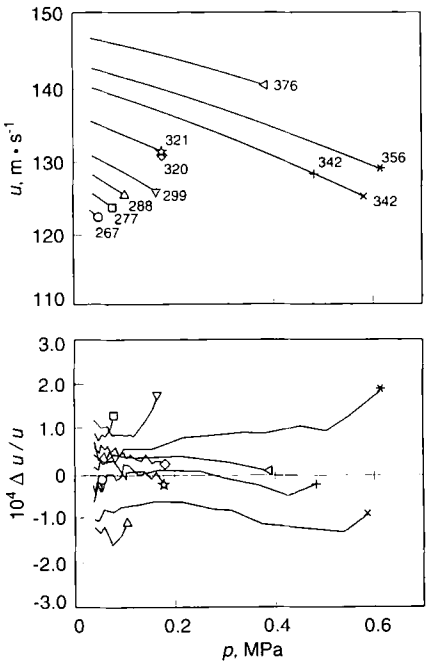

Fig. 13. Top: The speed of sound u in HFC-236ea as a function of p and T. Bottom: The deviations of u from the surface fit described in the text and the coefficients in Tables II and III. The label for each curve is the nominal temperature. $\Delta u/u \equiv (u_m - u_{fit})/u_{fit}$.

approximate. All of the isotherms were analyzed initially under the assumption that the molar mass of the sample was that of the pure compound, namely, 0.152039 kg · mol^{-1}. For the HFC-236ea-I data, this analysis gave an "effective" heat capacity $C^{\circ}_{p,\mathrm{I,eff}}$ which was in error by an amount given by Eq. (10). The HFC-236ea-I ideal-gas heat capacities were then corrected by the following scale factor:

$$C^{\circ}_{p\mathrm{I,adj}} = C^{\circ}_{p,\mathrm{I,eff}}[1 - (C^{\circ}_{p\mathrm{I,eff}}/R)\,f] \tag{18}$$

where $f = -1.218 \times 10^{-4}$ was chosen such that the deviations of $C^{\circ}_{p,\mathrm{I,adj}}$ and $C^{\circ}_{p\mathrm{II}}$ from a single fitted polynomial were the same for the two measurements near 320 K. The measured speed of sound $u_{\mathrm{I,m}}$ was adjusted in a manner that was consistent with Eq. (18) by

$$u_{\mathrm{I,adj}} = u_{\mathrm{I,m}}\sqrt{(1+f)} = 0.999939\,u_{\mathrm{I,m}} \tag{19}$$

The speed of sound and the standard deviation $\sigma[u]$ at each state point are given in Table A5. Figure 13 shows plots of u as a function of p

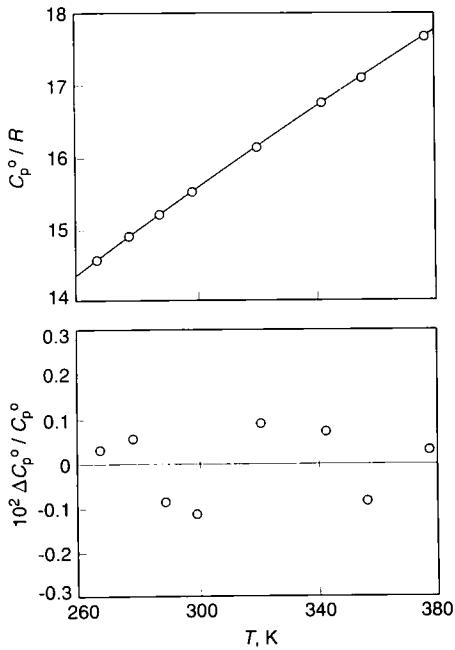

Fig. 14. Top: The measured ideal-gas heat capacity C°_{p} of HFC-236ea as a function of T. Bottom: The deviations of C°_{p} from Eq. (14). $\Delta C^{\circ}_{p}/C^{\circ}_{p} \equiv (C^{\circ}_{p,\mathrm{m}} - C^{\circ}_{p,\mathrm{fit}})/C^{\circ}_{p,\mathrm{fit}}$.

Table IX. Ideal-Gas Heat Capacity, Acoustic Virial Coefficients, and Density Virial Coefficients for HFC-236ea

T (K)	C_p^o (R)	$2\sigma[C_p^o]$ (R)	β_a ($cm^3 \cdot mol^{-1}$)	γ_a ($cm^3 \cdot mol^{-1} \cdot kPa^{-1}$)	$10^5\delta_a$ ($cm^3 \cdot mol^{-1} \cdot kPa^{-2}$)	B ($cm^3 \cdot mol^{-1}$)	$10^{-4}C$ ($cm^6 \cdot mol^{-2}$)	$10^{-8}D$ ($cm^9 \cdot mol^{-3}$)
267.150	14.598	0.020	−1788.1	−1.309		−1031.8	−158.06	−55.810
277.840	14.918	0.020	−1592.8	−1.035		−938.8	−71.85	−30.580
288.700	15.214	0.020	−1476.7	−0.528		−856.0	−28.15	−17.330
299.300	15.514	0.020	−1327.1	−0.489		−784.6	−7.11	−10.330
320.760	16.151	0.020	−1123.8	−0.250		−662.9	7.51	−3.990
321.118	16.161	0.025	−1119.8	−0.252	—			
342.432	16.743	0.022	−960.5	−0.108	−9.3	−563.8	9.09	−1.700
342.502			−962.5	−0.097	−10.8	—		
356.039	17.080	0.019	−872.5	−0.074	−5.9	−511.0	8.33	−1.050
376.903	17.643	0.021	−756.5	−0.045	−2.8	−441.1	6.74	−0.530

and the deviations from the surface fit for each isotherm. The ideal-gas heat capacities from isotherm fits are shown in Table IX. The heat capacities from HFC-236ea-II were fit separately to represent the most accurate data. In addition, the heat capacities of both samples were fit simultaneously. The results from both fits are included in Table II. Figure 14 shows the measured C_p^o and the deviations from Eq. (14) as a function of T. The acoustic virial coefficients, obtained from the isotherm fits, are given in Table IX. The number of coefficients that were significant at the 99.9% level is indicated by the number of entries in the table for each temperature. The surface $u(T, p)$ was fit with 11 adjustable parameters. The surface fit included the virial coefficients B, C, and D from which the acoustic virials β_a, γ_a, δ_a, and ε_a were calculated. The coefficient E was fixed at zero. Estimates of B, C, and D based on the fitted potential parameters are given in Table IX for several temperatures.

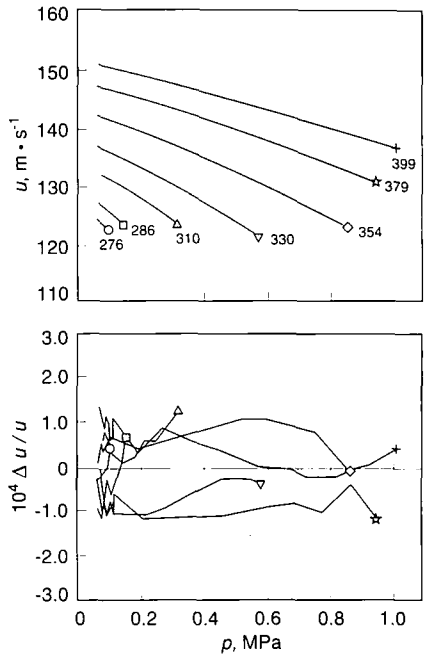

Fig. 15. Top: The speed of sound u in HFC-236fa as a function of p and T. Bottom: the deviations of u from the surface fit described in the text and the coefficients in Tables II and III. The label for each curve is the nominal temperature. $\Delta u/u \equiv (u_m - u_{fit})/u_{fit}$.

3.6. 1,1,1,3,3,3-Hexafluoropropane (HFC-236fa)

The acoustic measurements in HFC-236fa consisted of seven isotherms between 276 and 400 K. The pressure range for each isotherm was from 60 kPa to either 80% of the vapor pressure or 1000 kPa, whichever was lower. The temperatures of the gas handling system and the differential pressure transducer were maintained between 70 and 100°C to prevent condensation of the sample at high pressures during the acoustic measurements.

Gas chromatographic analysis indicated that the sample was 99.99% (by peak areas) pure HFC-236fa. No attempt was made to purify the sample further. As a precaution, the sample was degassed each time the sample was reused. The molar mass was assumed to be 0.152039 kg · mol^{-1} for the analysis of the acoustic measurements. Evidence that the gas composition changed was observed during the 400 K isotherm at the lowest

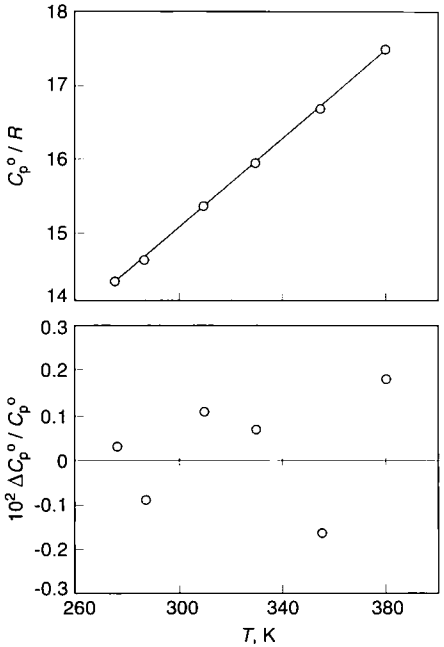

Fig. 16. Top: The measured ideal-gas heat capacity C_p° of HFC-236fa as a function of T. Bottom: The deviations of C_p° from Eq. (14). $\Delta C_p^\circ / C_p^\circ \equiv (C_{p,\mathrm{m}}^\circ - C_{p,\mathrm{fit}}^\circ)/C_{p,\mathrm{fit}}^\circ$.

pressures. This isotherm was not included in the fit to the ideal-gas heat capacities but was included in the surface fit.

The measured speed of sound u and the standard deviation $\sigma[u]$ at each state point are given in Table A6. Plots of u as a function of p and the deviation from the surface fit are shown in Fig. 15. The standard deviation in the speed of sound for the surface fit was 68 ppm. The surface fit favored coefficients for the ideal-gas heat capacity slightly different from those listed in Table II:

$$a_0 = 14.2634 \pm 0.047$$

$$a_1 = 0.029614 \pm 0.00013$$

The ideal-gas heat capacities, obtained from six of the seven isotherms, are given in Table X. Figure 16 shows the measured C_p° and the deviations from Eq. (14) as a function of T. The acoustic virial coefficients obtained

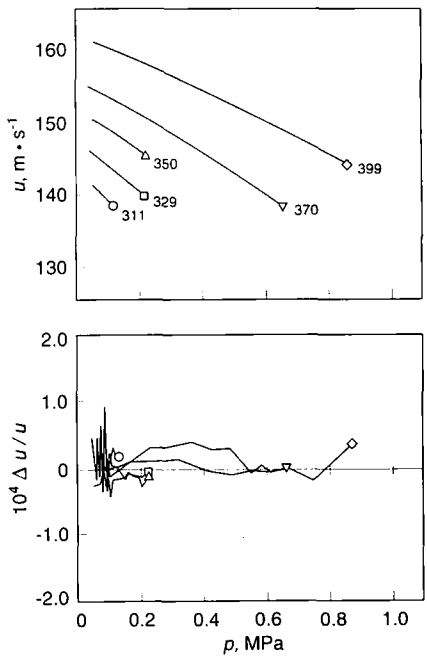

Fig. 17. Top: The speed of sound u in HFC-245ca as a function of p and T. Bottom: The deviations of u from the surface fit described in the text and the coefficients in Tables II and III. The label for each curve is the nominal temperature. $\Delta u/u \equiv (u_m - u_{fit})/u_{fit}$.

Table X. Ideal-Gas Heat Capacity, Acoustic Virial Coefficients, and Density Virial Coefficients for HFC-236fa

T (K)	C_p^o (R)	$2\sigma[C_p^o]$ (R)	β_a ($cm^3 \cdot mol^{-1}$)	γ_a ($cm^3 \cdot mol^{-1} \cdot kPa^{-1}$)	$10^5\delta_a$ ($cm^3 \cdot mol^{-1} \cdot kPa^{-2}$)	B ($cm^3 \cdot mol^{-1}$)	$10^{-4}C$ ($cm^6 \cdot mol^{-2}$)	$10^{-8}D$ ($cm^9 \cdot mol^{-3}$)
276.014	14.327	0.013	−1537.1	−0.9314		−905.6	−70.53	−3.491
286.975	14.640	0.011	−1402.9	−0.6328		−824.7	−35.42	−2.271
309.997	15.362	0.007	−1156.3	−0.3309		−684.4	−4.24	−0.996
329.995	15.958	0.003	−1011.3	−0.0923	−14.6	−587.5	3.81	−0.524
354.989	16.671	0.003	−841.2	−0.0473	−5.7	−489.6	6.02	−0.254
379.969	17.481	0.004	−706.7	−0.0259	−2.1	−411.0	5.62	−0.132
399.939			−609.9	−0.0309		−358.6	4.90	−0.081

from the isotherm fits are given in Table X. The surface $u(T, p)$ was fit with 11 adjustable parameters. The surface fit included the virial coefficients B, C, and D from which the acoustic virials β_a, γ_a, δ_a, and ε_a were calculated. The coefficient E was fixed at zero. Estimates of B, C, and D based on the fitted potential parameters are given in Table X for several temperatures.

3.7. 1,1,2,2,3-Pentafluoropropane (HFC-245ca)

The sound-speed Measurements in HFC-245ca consisted of five isotherms between 300 and 400 K and spanned the pressure range up 1000 kPa (or 80% of the vapor pressure, whichever was lower). Since the vapor pressure of HFC-245ca at 300 K is only about 100 kPa, the temperature of all the tubing and valves between the sample storage vessel and the fluid bath was maintained at about 100°C to prevent condensation at higher pressures. A thermostat kept the temperature of the DPT at about

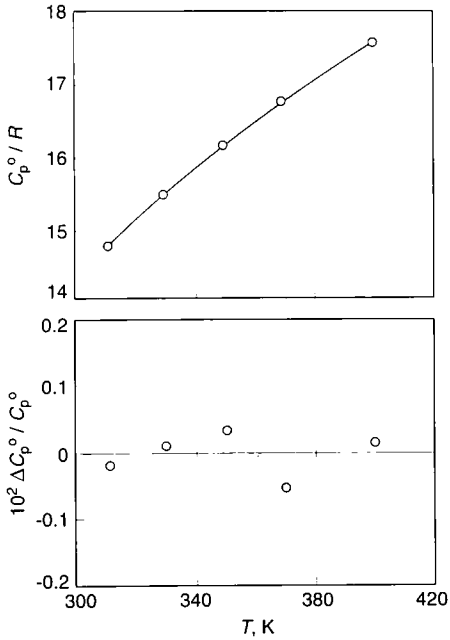

Fig. 18. Top: The measured ideal-gas heat capacity C_p° of HFC-245ca as a function of T. Bottom: The deviations of C_p° from Eq. (14). $\Delta C_p^\circ / C_p^\circ \equiv (C_{p,\mathrm{m}}^\circ - C_{p,\mathrm{fit}}^\circ)/C_{p,\mathrm{fit}}^\circ$.

Table XI. Ideal-Gas Heat Capacity, Acoustic Virial Coefficients, and Density Virial Coefficients for HFC-245ca

T (K)	C_p° (R)	$2\sigma[C_p^\circ]$ (R)	β_a ($cm^3 \cdot mol^{-1}$)	γ_a ($cm^3 \cdot mol^{-1} \cdot kPa^{-1}$)	$10^5\delta_a$ ($cm^3 \cdot mol^{-1} \cdot kPa^{-2}$)	B ($cm^3 \cdot mol^{-1}$)	$10^{-4}C$ ($cm^6 \cdot mol^{-2}$)	$10^{-8}D$ ($cm^9 \cdot mol^{-3}$)
311.374	14.744	0.024	−1438.9			−817.7	−20.64	−4.810
329.432	15.432	0.015	−1254.6	−0.3560		−710.3	−1.04	−2.880
350.014	16.110	0.021	−1051.9	−0.1660		−615.0	5.72	−1.710
369.998	16.697	0.023	−917.6	−0.0742	−8.7	−535.9	7.08	−1.050
399.959	17.508	0.019	−755.8	−0.0386	−3.3	−439.6	6.22	−0.520

100°C and controlled it to within ±0.1°C. The DPT had been recalibrated under these conditions.

Gas chromatographic analysis, based on peak-area ratios, showed the HFC-245ca sample to be 99.98% pure after degassing at 77 K. The impurity was not identified. The sample was sufficiently pure that no corrections to the speed of sound were necessary. Therefore, the molar mass was assumed to be 0.134049 kg · mol $^{-1}$ for the analysis of the acoustic data. During the handling of the sample, it was found that several Vacuum components containing nickel turned black after being in contact with the liquid. Reanalysis of the sample showed no significant change in the composition, however.

The measured speed of sound u and the standard deviation $\sigma[u]$ at each state point are given in Table A7. Figure 17 shows plots of u as a function of p and the deviations from the surface fit for each isotherm. The ideal-gas heat capacities are given in Table XI. Figure 18 shows the measured C_p^o and the deviations from Eq. (14) as a function of T. The acoustic virial coefficients, obtained from the isotherm fits, are given in Table XI. The surface $u(T, p)$ was fit with 11 adjustable parameters. The surface fit included the virial coefficients B, C, and D from which the acoustic virials β_a, γ_a, δ_a, and ε_a were calculated. The coefficient E was fixed at zero. Estimates of B, C, and D based on the fitted potential parameters are given in Table XI for several temperatures.

4. REMARKS

The fitted square-well parameters for the virial coefficients show notable trends among the compounds in this study (see Table III). Most importantly, none of the parameters have wildly variant values, which indicates that the fits do not contain an excessive number of parameters nor do they rely on a delicate cancellation of terms having comparable values. In fact, the λ's for the second virial coefficient B are approximately 1.3 for all the fluids. A closer inspection reveals that the parameters for B and C show systematic differences between the ethane- and the propane-based compounds with few exceptions. For example, note that the λ's for the propane-based compounds (HFC-236ea, HFC-236fa, and HFC-245ca) are systematically larger than the λ's for the ethane-based compounds (HCFC-124, HFC-125, HFC-143a, and HFC-152a). With the exception of HCFC-124, the λ's for the third virial coefficient C also show systematic differences between the ethane- and the propane-based compounds. The anomalous λ value for C for HCFC-124 could be an artifact, since C is the coefficient of the last term in the truncated virial expansion for this fluid, while D was included in the expansion for the other fluids.

ACKNOWLEDGMENTS

The author thanks Dana Defibaugh for his help in the GC analyses and in the purification of HFC-143a, Steven Boyes for providing his p–V–T data for comparison, and Mike Moldover for his stimulating and insightful ideas. This work was supported by U.S. Department of Energy Contract DE-A105-88ER13823, the Environmental Protection Agency (EPA DW13935432-01-4), and the U.S. Department of the Navy.

APPENDIX

Table A1. Speed of Sound in HCFC-124

p (kPa)	u ($m \cdot s^{-1}$)	$\sigma[u]\,u$ (ppm)
	$T = 250.010$ K	
36.80	127.836	16
34.21	127.964	15
30.45	128.160	11
27.05	128.330	10
24.07	128.484	11
21.41	128.608	41
	$T = 259.966$ K	
58.40	129.474	30
54.33	129.660	16
48.13	129.942	29
42.59	130.195	40
39.59	130.327	22
35.04	130.532	21
	$T = 269.908$ K	
88.36	130.867	50
78.06	131.299	37
72.50	131.530	27
64.08	131.875	13
56.65	132.176	23
46.36	132.591	10
38.02	132.922	50
31.15	133.192	21
15.01	133.817	50

Table A1. *(Continued)*

p (kPa)	u ($m \cdot s^{-1}$)	$\sigma[u]/u$ (ppm)
	$T = 279.871$ K	
100.28	133.114	50
100.21	133.117	50
92.31	133.415	27
86.02	133.646	50
79.29	133.897	25
73.82	134.097	11
64.73	134.429	13
63.41	134.475	10
52.72	134.865	14
52.43	134.872	12
40.86	135.285	21
39.18	135.344	11
14.78	136.201	50
	$T = 300.043$ K	
179.00	135.937	50
168.32	136.272	50
152.08	136.783	50
111.78	138.018	29
111.80	138.018	18
95.02	138.522	10
77.72	139.034	17
57.11	139.641	11
40.04	140.137	34
19.71	140.716	22
	$T = 319.675$ K	
442.48	133.948	17
378.20	135.827	12
308.87	137.769	10
240.38	139.612	16
170.78	141.416	11
102.46	143.127	10
	$T = 320.269$ K	
206.35	140.652	53
176.44	141.417	48
145.32	142.202	41
112.33	143.021	29
83.72	143.720	10
51.56	144.499	13
20.23	145.243	38

Table A1. *(Continued)*

p (kPa)	u ($m \cdot s^{-1}$)	$\sigma[u]/u$ (ppm)
	$T = 339.740$ K	
777.17	131.881	12
706.91	133.786	10
638.56	135.565	11
559.58	137.554	13
489.99	139.248	10
418.99	140.916	11
344.14	142.622	10
316.42	143.237	55
298.74	143.628	54
277.31	144.101	11
269.06	144.277	53
242.04	144.862	53
217.74	145.383	44
204.75	145.662	10
195.88	145.847	46
176.21	146.262	46
	$T = 340.221$ K	
294.02	143.856	1
265.90	144.469	52
240.40	145.019	51
203.82	145.797	46
172.93	146.446	41
146.63	146.994	34
112.63	147.695	23
83.70	148.284	10
55.70	148.850	12
54.11	148.883	14
39.74	149.172	21
29.68	149.368	52
	$T = 355.095$ K	
294.70	147.682	49
267.53	148.194	46
240.67	148.698	44
202.92	149.398	45
172.04	149.966	43
146.50	150.431	29
115.27	150.996	21
82.39	151.586	11
57.87	152.023	12
55.86	152.060	26
55.88	152.060	22
20.32	152.684	51

Table A1. *(Continued)*

p (kPa)	u ($m \cdot s^{-1}$)	$\sigma[u]/u$ (ppm)
	$T = 360.040$ K	
861.53	137.683	50
857.62	137.762	50
793.77	139.145	50
707.83	140.948	23
622.24	142.693	18
534.18	144.432	10
446.59	146.114	11
361.88	147.698	11
276.90	149.246	10
189.25	150.805	11
102.71	152.303	14
	$T = 365.000$ K	
295.10	150.140	57
275.48	150.478	52
247.12	150.964	46
213.32	151.541	43
191.33	151.912	39
160.06	152.438	37
134.18	152.870	23
104.82	153.357	15
79.11	153.782	10
49.55	154.267	19
19.85	154.751	65
	$T = 374.900$ K	
295.10	152.516	44
264.60	153.000	48
236.69	153.438	49
204.28	153.945	44
172.98	154.430	37
143.97	154.878	28
115.48	155.315	16
82.78	155.814	10
52.03	156.279	24
50.88	156.295	34
34.68	156.541	42
20.11	156.756	56
	$T = 380.120$ K	
861.55	144.582	70
826.66	145.188	14
734.57	146.747	11

Table A1. *(Continued)*

p (kPa)	u ($m \cdot s^{-1}$)	$\sigma[u]/u$ (ppm)
649.93	148.153	10
560.83	149.597	11
467.63	151.086	11
376.99	152.493	23
285.79	153.886	12
193.18	155.281	78
102.82	156.601	10
	$T = 385.650$ K	
295.60	155.020	56
270.06	155.389	47
233.66	155.912	46
209.94	156.249	33
173.99	156.761	23
144.70	157.176	19
115.42	157.587	15
82.40	158.051	17
51.62	158.478	16
	$T = 399.933$ K	
294.18	158.285	50
273.05	158.557	50
242.26	158.950	50
215.18	159.296	50
191.08	159.602	50
159.67	159.999	50
131.87	160.349	50
104.41	160.694	50
76.71	161.040	50
50.53	161.366	50
50.57	161.368	50
30.71	161.606	50
19.96	161.743	50
	$T = 400.045$ K	
874.59	150.481	50
781.36	151.791	38
717.79	152.673	52
635.82	153.793	42
560.04	154.814	43
481.43	155.862	37
402.90	156.896	41
321.07	157.958	34
243.64	158.952	26
163.07	159.977	16

Table A2. Speed of Sound in HFC-125

p (kPa)	u_m ($m \cdot s^{-1}$)	u_{125} ($m \cdot s^{-1}$)	$\sigma[u_m]/u_m$ (ppm)
	$T = 240.007$ K		
164.74	129.984	130.014	57
155.34	130.354	130.384	73
147.36	130.661	130.691	46
133.65	131.183	131.213	69
118.89	131.738	131.768	21
104.14	132.278	132.308	48
101.13	132.390	132.420	44
98.21	132.497	132.527	50
95.37	132.602	132.632	41
92.63	132.702	132.733	46
92.62	132.699	132.730	60
86.48	132.921	132.952	33
86.20	132.933	132.963	32
86.03	132.934	132.964	38
85.92	132.940	132.971	50
85.86	132.943	132.974	64
82.02	133.081	133.112	58
70.76	133.482	133.513	34
64.30	133.714	133.745	44
53.12	134.113	134.144	41
39.82	134.567	134.598	26
	$T = 260.023$ K		
162.91	136.571	136.602	48
154.23	136.822	136.853	52
145.99	137.063	137.094	45
138.17	137.288	137.320	45
125.68	137.647	137.678	52
118.90	137.839	137.870	43
107.52	138.159	138.190	41
97.65	138.439	138.470	41
88.66	138.690	138.721	42
80.11	138.931	138.963	54
80.10	138.931	138.962	37
68.44	139.251	139.282	37
61.81	139.435	139.467	35
50.38	139.752	139.784	79
38.85	140.058	140.089	51

Table A2. *(Continued)*

p (kPa)	u_m (m·s^{-1})	u_{125} (m·s^{-1})	$\sigma[u_m]/u_m$ (ppm)
	$T = 279.988$ K		
659.33	129.484	129.513	92
614.81	130.816	130.845	87
549.47	132.696	132.727	79
485.54	134.461	134.491	72
422.84	136.127	136.158	67
358.70	137.772	137.803	64
294.76	139.358	139.389	61
231.10	140.886	140.918	56
166.75	142.386	142.418	52
114.42	143.574	143.606	50
114.41	143.576	143.608	42
102.87	143.832	143.864	50
87.21	144.183	144.216	27
78.42	144.378	144.411	38
78.42	144.376	144.409	46
70.47	144.555	144.588	46
59.64	144.790	144.823	38
50.53	144.986	145.019	37
38.55	145.248	145.281	40
	$T = 300.003$ K		
999.09	129.895	129.925	158
910.40	132.148	132.178	150
823.95	134.246	134.277	103
718.30	136.692	136.722	93
613.67	139.004	139.035	82
513.12	141.133	141.165	76
408.11	143.272	143.305	72
307.47	145.247	145.280	66
204.51	147.201	147.234	56
102.55	149.074	149.108	46
102.55	149.075	149.108	47
86.10	149.370	149.404	46
76.94	149.538	149.571	45
64.64	149.758	149.792	43
51.71	149.985	150.019	39

Table A2. *(Continued)*

p (kPa)	u_m ($m \cdot s^{-1}$)	u_{125} ($m \cdot s^{-1}$)	$\sigma[u_m]/u_m$ (ppm)
	$T = 319.988$ K		
1023.02	138.714	138.746	179
840.16	142.079	142.111	86
840.06	142.081	142.113	133
778.98	143.159	143.192	86
778.69	143.164	143.196	88
778.57	143.168	143.200	89
692.81	144.655	144.687	82
606.22	146.115	146.148	79
521.14	147.526	147.560	78
435.92	148.905	148.939	70
348.60	150.294	150.328	53
264.25	151.603	151.637	56
178.36	152.912	152.946	52
103.27	154.038	154.073	42
99.93	154.090	154.125	40
96.19	154.146	154.181	43
92.67	154.199	154.234	47
89.28	154.244	154.279	53
89.29	154.248	154.282	60
65.17	154.606	154.641	51
40.22	154.970	155.005	54
	$T = 340.003$ K		
1006.52	146.814	146.847	108
911.58	148.168	148.201	92
810.91	149.576	149.610	83
720.79	150.815	150.849	80
506.62	153.684	153.718	66
405.17	155.007	155.042	58
305.88	156.281	156.316	54
201.87	157.595	157.631	51
173.77	157.945	157.981	48
136.72	158.407	158.443	45
77.99	159.137	159.172	43
59.95	159.359	159.395	51

Table A2. *(Continued)*

p (kPa)	u_m (m·s^{-1})	u_{125} (m·s^{-1})	$\sigma[u_m]/u_m$ (ppm)
	$T = 359.958$ K		
1002.01	153.667	153.702	99
911.46	154.695	154.730	97
802.37	155.917	155.952	88
707.54	156.969	157.005	79
615.98	157.972	158.008	70
500.47	159.225	159.260	67
411.29	160.181	160.217	62
306.30	161.293	161.329	57
203.80	162.371	162.407	57
102.64	163.422	163.459	48
102.65	163.423	163.460	45
93.79	163.517	163.554	39
83.28	163.624	163.661	40
72.53	163.738	163.775	36
61.70	163.848	163.885	48
51.57	163.954	163.991	36
42.75	164.043	164.080	24
	$T = 379.983$ K		
999.32	159.845	159.881	96
922.66	160.552	160.588	94
821.68	161.473	161.509	86
717.61	162.419	162.455	82
613.97	163.353	163.390	79
513.91	164.251	164.288	69
411.33	165.164	165.201	59
307.72	166.077	166.114	61
205.32	166.978	167.016	43
130.15	167.636	167.673	40
130.13	167.638	167.675	42
120.76	167.718	167.756	49
112.06	167.794	167.832	43
98.23	167.911	167.948	50
91.15	167.973	168.011	43
79.97	168.071	168.109	35
70.16	168.157	168.195	33
60.11	168.238	168.275	38
48.98	168.331	168.369	26
39.29	168.417	168.455	55

Table A2. *(Continued)*

p (kPa)	u_m (m·s^{-1})	u_{125} (m·s^{-1})	$\sigma[u_m]\ u_m$ (ppm)
	$T = 400.000$ K		
1016.43	165.369	165.406	68
935.97	165.999	166.036	46
826.68	166.822	166.859	40
725.01	167.582	167.619	47
625.62	168.325	168.362	59
519.17	169.119	169.157	44
415.18	169.890	169.928	51
312.06	170.657	170.695	38
207.03	171.433	171.472	32

Table A3. Speed of Sound in HCFC-143a

p (kPa)	u (m·s^{-1})	$\sigma[u]\ u$ (ppm)
	$T = 250.011$ K	
229.27	158.178	69
220.72	158.563	68
204.04	159.306	59
190.34	159.908	69
176.22	160.522	55
159.91	161.222	55
145.43	161.837	53
132.59	162.377	42
117.88	162.990	33
102.22	163.633	38
	$T = 250.026$ K	
131.87	162.428	48
126.10	162.668	41
114.68	163.139	35
104.17	163.569	29
94.65	163.957	29
82.45	164.450	22
72.22	164.863	10
63.95	165.190	12
53.85	165.594	28

Table A3. *(Continued)*

p (kPa)	u (m · s^{-1})	$\sigma[u]$ u (ppm)
	$T = 289.962$ K	
588.58	163.138	66
435.26	167.746	46
350.69	170.154	53
269.18	172.402	55
183.23	174.702	40
165.33	175.181	31
103.28	176.799	16
	$T = 309.997$ K	
858.88	165.273	32
858.88	165.273	32
775.18	167.428	49
703.11	169.237	55
633.58	170.931	51
532.72	173.335	58
429.27	175.726	62
323.07	178.110	53
218.41	180.399	47
	$T = 319.438$ K	
1007.24	166.339	31
916.97	168.474	47
814.31	170.838	31
707.63	173.216	40
613.54	175.261	58
510.08	177.457	46
407.29	179.581	42
309.78	181.552	34
205.67	183.615	31
102.39	185.620	23
	$T = 339.913$ K	
1007.27	175.969	80
918.08	177.597	54
824.14	179.286	36
708.87	181.318	58
609.28	183.034	92
518.05	184.597	71
402.52	186.537	81
309.19	188.080	60
203.18	189.805	42
102.20	191.435	5

Table A3. *(Continued)*

p (kPa)	u (m · s $^{-1}$)	$\sigma[u]\,u$ (ppm)
	$T = 359.985$ K	
986.13	184.505	27
905.70	185.702	243
826.63	186.851	69
737.54	188.124	47
652.23	189.343	50
560.98	190.631	60
466.28	191.953	61
375.85	193.203	58
281.27	194.502	48
194.54	195.685	31
102.02	196.939	2
	$T = 379.998$ K	
1014.19	191.501	89
939.72	192.403	47
816.99	193.867	90
719.88	195.022	95
626.19	196.127	83
520.04	197.374	56
413.81	198.611	52
308.20	199.834	48
202.94	201.050	30
100.06	202.236	6
	$T = 399.979$ K	
1011.21	198.340	31
922.19	199.229	35
832.87	200.120	58
712.65	201.313	78
610.01	202.328	89
503.29	203.384	61
409.72	204.305	58
306.50	205.321	44
207.62	206.291	27
104.16	207.312	3

Table A4. Speed of Sound in HCFC-152a

p (kPa)	u (m · s^{-1})	$\sigma[u]\cdot u$ (ppm)
	$T = 242.776$ K	
65.18	184.616	28
62.95	184.763	33
59.21	184.997	12
55.69	185.214	12
51.44	185.485	7
48.38	185.659	23
44.72	185.893	84
	$T = 273.130$ K	
208.59	189.826	89
194.02	190.505	79
175.29	191.369	65
154.41	192.313	58
136.22	193.126	42
117.45	193.951	28
97.20	194.829	13
79.14	195.599	12
59.46	196.428	4
40.72	197.215	77
	$T = 289.946$ K	
379.12	190.130	101
344.60	191.579	100
292.27	193.666	101
264.48	194.747	101
238.98	195.727	101
218.13	196.500	105
163.24	198.548	48
133.59	199.628	27
94.87	201.019	18
89.18	201.215	9
79.23	201.567	2
73.75	201.740	12
66.39	202.016	30
60.03	202.242	25
53.59	202.439	91
47.99	202.663	25
40.67	202.948	34
	$T = 300.013$ K	
473.88	191.382	90
438.84	192.716	58

Table A4. *(Continued)*

p (kPa)	u ($m \cdot s^{-1}$)	$\sigma[u]\,u$ (ppm)
398.76	194.202	50
359.03	195.640	48
314.27	197.225	44
268.53	198.807	39
226.97	200.212	41
185.61	201.586	32
145.99	202.876	29
125.63	203.532	26
125.68	203.531	26
108.78	204.071	25
101.68	204.292	27
101.67	204.293	27
98.77	204.390	31
95.64	204.485	26
89.65	204.680	34
87.60	204.739	29
80.94	204.949	30
77.14	205.075	30
74.31	205.156	23
68.33	205.350	16
61.73	205.557	13
54.90	205.759	35
47.17	206.008	5
40.81	206.207	12
	$T = 309.991$ K	
667.80	189.465	83
501.48	195.330	25
480.44	196.051	86
419.40	198.061	84
362.51	199.883	81
232.55	203.881	57
163.94	205.912	43
98.96	207.798	33
93.35	207.957	24
86.93	208.139	1
80.31	208.325	2
56.32	209.009	37
50.70	209.173	25
46.74	209.287	63
41.97	209.421	25
38.79	209.513	25

Table A4. *(Continued)*

p (kPa)	u (m · s^{-1})	$\sigma[u]/u$ (ppm)
	$T = 329.945$ K	
1029.78	188.822	60
821.19	195.317	77
631.81	200.761	78
557.90	202.779	72
454.70	205.517	74
368.36	207.735	61
276.42	210.035	48
185.20	212.259	40
120.13	213.818	8
103.52	214.195	37
96.55	214.360	4
89.41	214.539	4
86.32	214.605	0
75.98	214.848	9
75.63	214.863	10
65.19	215.113	6
63.26	215.156	18
58.08	215.272	23
51.74	215.421	43
45.64	215.566	52
39.97	215.694	35
	$T = 349.990$ K	
1014.58	200.589	120
913.80	203.009	84
531.16	211.654	71
449.68	213.383	93
363.69	215.189	71
309.61	216.295	58
182.80	218.881	15
93.87	220.644	4
93.92	220.636	3
87.44	220.767	1
82.23	220.870	13
74.76	221.017	16
68.07	221.150	16
50.95	221.499	3
50.92	221.509	32
46.67	221.595	25
34.70	221.856	25

Table A4. *(Continued)*

p (kPa)	u ($m \cdot s^{-1}$)	$\sigma[u]/u$ (ppm)
	$T = 369.985$ K	
1016.46	210.144	54
799.81	214.262	67
611.98	217.688	80
445.39	220.631	96
189.75	225.036	62
104.79	226.467	0
98.46	226.577	3
94.53	226.641	7
87.67	226.758	9
82.42	226.851	18
76.49	226.948	16
69.41	227.064	12
62.28	227.189	57
56.50	227.284	35
47.64	227.432	48
41.07	227.549	25
	$T = 399.959$ K	
1005.18	222.780	58
955.63	223.487	63
947.80	223.601	67
947.77	223.599	57
947.64	223.602	54
820.09	225.402	76
505.23	229.767	70
459.75	230.391	62
375.46	231.534	54
335.84	232.069	50
204.09	233.838	16
107.55	235.122	3
106.93	235.133	7
97.36	235.262	9
92.53	235.329	6
87.86	235.393	16
82.24	235.469	17
82.08	235.473	12

Table A5. Speed of Sound in HCFC-236ea

p (kPa)	u ($m \cdot s^{-1}$)	$\sigma[u]/u$ (ppm)
	$T = 267.150$ K	
55.44	122.293	20
52.75	122.441	50
50.18	122.586	27
47.73	122.721	20
45.40	122.847	30
43.22	122.967	29
41.12	123.081	46
39.10	123.191	59
37.18	123.295	23
	$T = 277.840$ K	
80.85	123.815	49
75.01	124.107	44
68.38	124.434	38
59.28	124.878	34
54.04	125.131	39
46.79	125.476	37
40.48	125.775	32
	$T = 288.700$ K	
106.70	125.487	49
97.22	125.910	46
88.48	126.293	48
76.43	126.816	58
69.56	127.112	35
60.00	127.522	27
49.56	127.958	32
40.97	128.316	27
	$T = 299.300$ K	
170.28	125.724	58
161.67	126.083	57
153.38	126.426	56
145.56	126.747	52
138.02	127.052	52
130.93	127.338	52
124.17	127.608	50
117.80	127.861	52
107.46	128.270	44
101.91	128.487	48
101.91	128.487	46
92.89	128.837	46

Table A5. *(Continued)*

p (kPa)	u ($m \cdot s^{-1}$)	$\sigma[u]/u$ (ppm)
88.04	129.024	39
79.90	129.336	45
75.67	129.496	44
68.66	129.764	35
58.98	130.127	30
53.48	130.332	41
45.92	130.614	42
39.47	130.851	47
	$T = 320.760$ K	
181.13	131.203	58
171.30	131.521	56
162.07	131.819	53
153.23	132.100	53
144.84	132.369	55
136.89	132.618	53
129.36	132.855	53
122.22	133.078	46
110.41	133.445	46
104.28	133.634	47
98.48	133.814	47
92.94	133.982	47
87.80	134.139	50
82.89	134.291	43
74.82	134.535	38
67.56	134.756	34
60.94	134.953	32
54.97	135.133	46
46.77	135.373	38
42.21	135.511	64
	$T = 321.118$ K	
178.65	131.371	53
172.88	131.558	55
163.55	131.859	58
154.99	132.130	52
146.94	132.386	52
137.35	132.688	50
128.35	132.969	49
119.99	133.229	51
111.25	133.501	43
101.68	133.795	44
101.68	133.795	44
95.03	133.996	49

Table A5. *(Continued)*

p (kPa)	u (m·s^{-1})	$\sigma[u]/u$ (ppm)
89.05	134.180	45
81.52	134.410	29
73.69	134.647	44
66.59	134.860	21
60.17	135.051	27
54.37	135.226	50
46.43	135.457	64
39.67	135.659	7
	$T = 342.432$ K	
487.94	127.977	82
427.34	129.813	74
375.84	131.321	74
321.22	132.867	70
261.46	134.503	57
212.37	135.807	61
157.01	137.239	55
101.10	138.647	36
101.09	138.645	43
94.61	138.808	41
88.51	138.958	41
81.35	139.134	44
74.77	139.299	49
66.90	139.493	35
61.60	139.620	42
53.22	139.822	55
47.79	139.957	24
40.10	140.138	64
	$T = 342.502$ K	
586.96	124.809	84
540.31	126.334	85
485.47	128.064	80
436.42	129.555	73
375.51	131.340	73
322.14	132.851	66
263.78	134.448	62
211.94	135.826	61
158.54	137.207	55
102.49	138.617	42
102.49	138.617	40
95.95	138.780	47
88.47	138.965	41
81.65	139.132	45
75.44	139.285	46

Table A5. *(Continued)*

p (kPa)	u ($m \cdot s^{-1}$)	$\sigma[u]/u$ (ppm)
68.06	139.467	49
61.54	139.627	48
54.32	139.802	51
46.98	139.979	18
41.12	140.122	12
	$T = 356.039$ K	
615.17	128.965	85
554.72	130.624	83
502.97	132.000	84
456.73	133.202	78
392.57	134.818	72
336.58	136.191	68
272.05	137.727	62
219.30	138.952	57
157.04	140.362	54
99.79	141.633	56
99.77	141.633	57
93.88	141.760	47
88.34	141.882	41
79.29	142.079	49
74.55	142.182	38
66.89	142.348	41
60.02	142.500	51
53.87	142.632	40
45.49	142.808	52
40.86	142.909	31
	$T = 376.904$ K	
388.55	140.466	69
330.45	141.614	61
280.64	142.582	57
217.04	143.795	56
157.86	144.904	51
101.86	145.936	42
101.86	145.936	45
94.38	146.074	40
87.39	146.201	50
80.99	146.314	72
73.06	146.463	35
67.70	146.559	45
61.13	146.677	28
53.44	146.818	54
46.75	146.938	52
40.49	147.055	22

Table A6. Speed of Sound in HCFC-236fa

p (kPa)	u (m·s^{-1})	$\sigma[u]/u$ (ppm)
	$T = 276.014$ K	
97.96	122.878	49
95.97	122.976	50
91.17	123.212	54
88.19	123.357	47
83.89	123.567	54
77.03	123.898	43
73.24	124.078	58
69.67	124.249	53
66.24	124.411	40
60.47	124.681	54
	$T = 286.975$ K	
150.92	123.482	98
142.27	123.874	87
133.80	124.255	78
123.20	124.726	53
113.42	125.154	50
101.73	125.659	54
91.19	126.113	76
81.77	126.505	59
71.88	126.925	11
61.68	127.345	25
	$T = 309.997$ K	
319.45	123.647	73
245.31	126.478	51
213.02	127.654	62
178.12	128.881	61
138.58	130.232	54
102.17	131.442	66
102.17	131.445	55
94.57	131.694	55
84.37	132.026	43
75.52	132.307	23

Table A6. *(Continued)*

p (kPa)	u (m · s^{-1})	$\sigma[u]/u$ (ppm)
	$T = 329.995$ K	
580.59	121.302	68
545.06	122.585	75
503.52	124.036	82
454.85	125.678	75
376.91	128.185	84
326.68	129.730	87
275.51	131.253	80
219.40	132.869	87
165.72	134.367	81
	$T = 329.995$ K	
109.90	135.881	72
109.90	135.880	64
106.33	135.979	96
100.85	136.125	62
95.59	136.262	55
88.90	136.441	41
82.81	136.602	43
78.70	136.708	61
72.61	136.869	37
66.98	137.022	41
61.78	137.161	10
	$T = 354.989$ K	
864.46	122.729	61
759.04	125.782	71
662.06	128.430	90
594.62	130.195	99
533.35	131.748	57
456.37	133.635	66
277.86	137.778	61
194.12	139.622	53
101.41	141.607	12
78.94	142.075	9
73.93	142.178	38
70.58	142.250	2
66.05	142.341	2
61.67	142.429	24

Table A6. *(Continued)*

p (kPa)	u (m·s^{-1})	$\sigma[u]/u$ (ppm)
	$T = 379.969$ K	
946.79	130.705	63
867.01	132.419	80
773.01	134.357	50
681.65	136.193	95
580.85	138.153	52
514.70	139.407	51
454.81	140.521	65
299.53	143.330	60
204.85	144.987	56
109.26	146.631	10
105.65	146.686	50
101.95	146.748	83
98.38	146.809	66
91.32	146.928	68
88.30	146.977	68
82.28	147.080	20
76.89	147.172	7
71.74	147.255	13
61.70	147.426	50
	$T = 399.939$ K	
1014.54	136.474	53
921.75	138.054	56
862.51	139.046	51
813.38	139.856	63
729.74	141.219	43
682.48	141.980	67
591.81	143.414	10
518.61	144.554	64
454.45	145.540	50
345.92	147.178	52
266.02	148.364	52
187.85	149.494	52
110.93	150.611	33
110.93	150.607	52
106.79	150.664	85
100.14	150.758	90
96.12	150.822	29
90.18	150.908	62
82.44	151.014	23
77.54	151.089	17
72.75	151.158	25
67.43	151.234	42

Table A7. Speed of Sound in HCFC-245ca

p (kPa)	u ($m \cdot s^{-1}$)	$\sigma[u]/u$ (ppm)
	$T = 311.374$ K	
131.59	138.399	41
124.77	138.699	32
118.04	138.995	27
109.21	139.375	46
101.31	139.712	44
94.00	140.024	34
86.46	140.341	91
70.01	141.025	3
62.93	141.319	25
	$T = 329.987$ K	
230.96	139.698	58
218.76	140.168	53
206.58	140.633	66
192.05	141.185	58
174.35	141.846	42
162.03	142.299	42
156.24	142.510	44
147.07	142.842	50
138.36	143.158	33
130.16	143.453	17
120.96	143.779	42
110.19	144.162	14
102.81	144.421	5
102.82	144.418	3
95.81	144.662	20
87.71	144.944	13
80.26	145.200	20
73.48	145.431	39
66.08	145.683	48
51.25	146.194	50
	$T = 350.014$ K	
232.79	145.354	65
223.62	145.638	50
204.94	146.211	61
191.31	146.626	52
178.52	147.011	46
163.61	147.458	35
150.02	147.860	45

Table A7. *(Continued)*

p (kPa)	u ($m \cdot s^{-1}$)	$\sigma[u]/u$ (ppm)
133.64	148.342	35
119.12	148.766	23
104.35	149.190	42
104.35	149.198	23
97.49	149.393	27
93.60	149.505	29
87.55	149.686	31
81.83	149.836	0
75.25	150.039	10
61.63	150.416	4
51.04	150.728	35
	$T = 369.998$ K	
673.31	137.958	5
613.97	139.859	32
559.50	141.537	28
485.50	143.735	50
438.03	145.092	35
367.43	147.048	40
298.35	148.892	48
234.17	150.552	51
169.60	152.173	42
105.60	153.736	7
105.60	153.736	56
99.57	153.882	28
94.05	154.012	48
86.78	154.190	12
82.21	154.304	52
77.68	154.416	61
77.67	154.406	62
51.28	155.034	50
	$T = 399.959$ K	
876.47	143.734	55
751.55	146.740	33
675.75	148.494	12
619.85	149.749	31
549.85	151.285	36
496.73	152.423	41
399.55	154.453	46
320.22	156.065	48
250.89	157.439	51
176.50	158.884	29
102.23	160.295	31
102.23	160.299	9
96.78	160.404	34
90.65	160.528	31
85.32	160.624	35
80.19	160.704	2
75.40	160.809	23
67.53	160.951	50
63.85	160.013	78

REFERENCES

1. M. R. Moldover, M. Waxman, and M. Greenspan, *High Temp. High Press.* **11**:75 (1979).
2. J. B. Mehl and M. R. Moldover, *J. Chem. Phys.* **74**:4062 (1981).
3. J. B. Mehl and M. R. Moldover, in *Proc. Eighth Symp. Thermophys. Prop.* J. V. Sengers, ed. (ASME, New York, 1982), pp. 134–141.
4. M. R. Moldover, J. B. Mehl, and M. Greenspan, *J. Acoust. Soc. Am.* **79**:253 (1986).
5. M. R. Moldover, J. P. M. Trusler, T. J. Edwards, J. B. Mehl, and R. S. Davis, *J. Res. Natl. Bur. Stand.* **93**:85 (1988).
6. J. P. M. Trusler, *Physical Acoustics and Metrology of Fluids* (Adam Hilger, Bristol, 1991).
7. *NIST Thermodynamic Properties of Refrigerants and Refrigerant Mixtures*, NIST Standard Reference Database 23 (Standard Reference Data Program, NIST, Gaithersburg, MD).
8. A. R. H. Goodwin and M. R. Moldover, *J. Chem. Phys.* **93**:2741 (1990).
9. A. R. H. Goodwin and M. R. Moldover, *J. Chem. Phys.* **95**:5230 (1991).
10. A. R. H. Goodwin and M. R. Moldover, *J. Chem. Phys.* **95**:5236 (1991).
11. Apparatus for Acoustic Measurements of Gases with Applications for High K. A. Gillis and M. R. Moldover, in *Proceedings of the Ninth Symposium on Energy Engineering Sciences* (Argonne National Laboratory, May 13–15, 1991), p. 310.
12. D. Defibaugh, K. A. Gillis, M. R. Moldover, G. Morrison, and J. W. Schmidt, *Fluid Phase Equil.* **81**:285 (1992).
13. K. A. Gillis, *Int. J. Thermophys.* **15**:821 (1994).
14. K. A. Gillis, A. R. H. Goodwin, and M. R. Moldover, *Rev. Sci Instrum.* **62**:2213 (1991).
15. W. Van Dael, in *IUPAC Series in Experimental Thermodynamics, Vol. 2: Experimental Thermodynamics of Non-reacting Fluids*, B. Le Neindré and B. Vodar, eds. (Butterworths, London, 1975), Chap. 11.
16. K. A. Gillis and M. R. Moldover, *Int. J. Thermophys.* **17**:1305 (1996).
17. J. P. M. Trusler and M. Zarari, *J. Chem. Thermodyn.* **24**:973 (1992).
18. G. C. Maitland, M. Rigby, E. B. Smith, and W. A. Wakeham, *Intermolecular Forces* (Clarendon Press, Oxford, 1981).
19. E. M. Sevick and P. A. Monson, *J. Chem. Phys.* **94**:3070 (1991).
20. J. W. S. Rayleigh, *Theory of Sound* (Dover, New York, 1945).
21. R. C. Reid, J. M. Prausnitz, and B. E. Poling, *The Properties of Gases and Liquids*, 4th ed. (McGraw-Hill, New York, 1987), Chaps. 9, 10.
22. D. Reichenberg, *AIChE J.* **21**:181 (1975).
23. S. J. Boyes and L. A. Weber, *Int. J. Thermophys.* **15**:443 (1994).
24. *TRC Thermodynamic Tables—Non-Hydrocarbons*, Table v-6881, J. Chao and A. S. Rodgers, compilers (Thermodynamics Research Center, The Texas A&M University System, College Station, 1989).
25. S. S. Chen, A. S. Rodgers, J. Chao, R. C. Wilhoit, and B. J. Zwolinski, *J. Chem. Ref. Data* **4**:441 (1975).
26. D. A. Compton and D. M. Rayner, *J. Phys. Chem.* **86**:1628 (1982).
27. B. Beagley, M. O. Jones, and P. Yavari, *J. Mol. Struct.* **71**:203 (1981).
28. C. M. Bignell and P. J. Dunlop, *J. Chem. Phys.* **98**:4889 (1993).
29. S. J. Boyes and L. Weber, *J. Chem. Thermodyn.* **27**:163 (1995).
30. T. J. Buckley and K. A. Gillis, *J. Chromatogr. A* **702**:243 (1995).